ATMOSPHERIC ENVIRONMENT: X 6 (2020) 100073

Contents lists available at ScienceDirect

Atmospheric Environment: X

journal homepage: http://www.journals.elsevier.com/atmospheric-environment-x

Large-eddy simulation of the optimal street-tree layout for pedestrian-level aerosol particle concentrations – A case study from a city-boulevard

Sasu Karttunen [a,*,1], Mona Kurppa [a,**,1], Mikko Auvinen [b], Antti Hellsten [b], Leena Järvi [a,c]

[a] Institute for Atmospheric and Earth System Research/Physics, Faculty of Science, 00014, University of Helsinki, Finland
[b] Finnish Meteorological Institute, 00101, Helsinki, Finland
[c] Helsinki Institute of Sustainability Science, Faculty of Science, 00014, University of Helsinki, Finland

ARTICLE INFO

Keywords:
CFD
LES
Pollutant dispersion
Street canyon
Urban vegetation
Urban ventilation

ABSTRACT

Street vegetation has been found to have both positive and negative impacts on pedestrian-level air quality, but the net effect has remained unclear. In this study, the effect of street trees on aerosol mass (PM_{10} and $PM_{2.5}$) and number in a boulevard-type street canyon with high traffic volumes in Helsinki is examined using the large-eddy simulation model PALM. Including a detailed aerosol module and a canopy module to comprise permeable trees, PALM allows to examine the effect of street trees in depth. The main aim is to understand the relative importance of dry deposition and the aerodynamic impact of street trees on the different aerosol measures at pedestrian-level and to find a suitable street-tree layout that would minimise the pedestrian-level aerosol particle concentrations over the boulevard pavements. The layout scenarios were decided together with urban planners who needed science-based knowledge to support the building of new neighbourhoods with boulevard-type streets in Helsinki. Two wind conditions with wind being parallel and perpendicular to the boulevard under neutral atmospheric stratification are examined.

Adding street trees to the boulevard increases aerosol particle concentrations on the pavements up to 123%, 72% and 53% for PM_{10}, $PM_{2.5}$ and total number, respectively. This shows decreased ventilation to be more important for local aerosol particle concentrations than dry deposition on vegetation. This particularly for PM_{10} and $PM_{2.5}$ whereas for aerosol number, dominated by small particles, the importance of dry deposition increases. Therefore the studied aerosol measure is important when the effect of vegetation on pedestrian-level air quality is quantified. Crown volume fraction in the street space is one of the main determining factors for elevated mass concentrations on the pavements. The lowest pedestrian-level mass concentrations are seen with three rows of trees of variable height, whereas the lowest number concentrations with four rows of uniform trees. The tree-height variation allows stronger vertical turbulent transport with parallel wind and largest volumetric flow rates with perpendicular wind. Introducing low (height < 1 m) hedges under trees between the traffic lanes and pavements is found to be a less effective mitigation method for particle mass than introducing tree-height variability, and for particle number less effective than maximising the tree volume in the street canyon.

The results show how street trees in a boulevard-type street canyon lead to decreased pedestrian-level air quality with the effect being particularly strong for larger aerosol particles. However, with careful planning of the street vegetation, significant reductions in pedestrian-level aerosol particle concentrations can be obtained.

1. Introduction

Road traffic is one of the main sources for urban air pollution (Fenger, 2009) and as a result the largest pollutant concentrations are commonly observed at pedestrian-level in street canyons with limited pollutant ventilation. Thus, for the well-being of urban dwellers, improvements particularly in street-canyon air quality are in a key role as people walk and cycle in the street space and the surrounding buildings

* Corresponding author.
** Corresponding author.
E-mail addresses: sasu.karttunen@helsinki.fi (S. Karttunen), mona.kurppa@helsinki.fi (M. Kurppa), mikko.auvinen@fmi.fi (M. Auvinen), antti.hellsten@fmi.fi (A. Hellsten), leena.jarvi@helsinki.fi (L. Järvi).
[1] These authors contributed equally to this work

https://doi.org/10.1016/j.aeaoa.2020.100073
Received 13 December 2019; Received in revised form 23 March 2020; Accepted 26 March 2020
Available online 7 April 2020

are generally occupied by residents.

Urban vegetation is often proposed as one mean to improve the pedestrian-level air quality by enhancing pollutant removal by dry deposition (e.g., Irga et al., 2015; Tallis et al., 2011). At the same time, trees decelerate the flow, modify turbulence and influence the canyon vortex (Gromke and Blocken, 2015; Raupach et al., 1996), which can deteriorate street canyon ventilation. However, the relative importance of these aforementioned aerodynamic impacts and dry deposition are not well-known and contradictory results on the influence of urban vegetation on pedestrian-level air quality have been published. For instance, Abhijith et al. (2017) concluded that introducing urban vegetation has been found to change pedestrian-level pollutant concentrations from −61% to +246%. Hence, while improving pedestrian-level thermal and wind comfort (Lindberg et al., 2016), health (Niemelä et al., 2010), and providing surface area for pollutant dry deposition (e.g., Janhäll, 2015), poorly positioned street trees can notably decrease pollutant ventilation and local air quality (Buccolieri et al., 2009, 2011; Gromke and Ruck, 2012).

Naturally, the most direct mean to lower the pedestrian-level pollutant concentrations is to reduce traffic emissions. However, even though combustion-related air pollutant emissions from traffic are likely to notably decrease within the next years, vehicular suspension of aerosol particles from brake and tyre wear might even increase as heavier electric cars will increase the load on pavement surface materials (Requia et al., 2018). Therefore, especially in countries where studded tyres are used, road dust is and will very probably remain a problem in future also. Traffic emission reductions will also take time and meanwhile alternative methods to decrease the pedestrian-level pollutant concentrations are needed. Highest pedestrian-level pollutant concentrations are especially detected when prevailing meteorological conditions and turbulent mixing lead to inefficient pollutant transport from the ground and mixing of clear air above (Britter and Hanna, 2003).

Pollutant transport has previously been found to be largely modified by urban form and morphology, described by factors such as building packing density (Lin et al., 2014; Yuan et al., 2014; Ramponi et al., 2015; Chen et al., 2017), building height variability (Hang et al., 2012), roof geometry (Nosek et al., 2016) and street canyon aspect ratios (Barlow et al., 2004). Vegetation has also been found to have considerable effect on local pollutant transport and concentrations (Buccolieri et al., 2009; Vos et al., 2013). As the effects of these urban properties for air quality are considerable, taking them into account in urban planning can lead to better pedestrian-level air quality (Kurppa et al., 2018).

To investigate the impact of individual trees and vegetation on the spatial and temporal variability of local air quality, high-resolution modelling that takes into account the complex interactions between the emissions, meteorological conditions, background concentrations and urban form is needed. Specifically, the used model should be capable of resolving the impact of single solid buildings and porous vegetation, for which computational fluid dynamics (CFD) is an optimal tool. Previous CFD studies combining the aerodynamic impact of vegetation and dry deposition show that dry deposition has a minor effect on aerosol concentrations compared to the aerodynamic impact (Jeanjean et al., 2016, 2017; Santiago et al., 2017a; Vos et al., 2013; Vranckx et al., 2015). Vegetation has mainly been shown to increase concentrations particularly in street canyons (around 5–6% in Jeanjean et al. (2017), 5% in Santiago et al. (2017a), 0.2–2.6% increase in PM_{10} in Vranckx et al. (2015)), while some studies show that vegetation can be a promising mitigation tool for air pollution (Jeanjean et al., 2016; Santiago et al., 2017b). Furthermore, local differences can be notable and even up to ±100% as shown by Santiago et al. (2017a). Concerning hedges, Janhäll (2015) concluded that (low) vegetation close to the emission source would be the best choice for enhancing aerosol dry deposition while not preventing street-canyon ventilation. Still, contradicting results exist and, for example Gromke et al. (2016) showed 3–19% higher and 18–60% lower pedestrian-level concentrations with discontinuous and continuous, respectively, hedge rows of 1.5–2.25 m in height. These results show how the impact of urban vegetation largely depends on the vegetation configuration and the site being studied.

However, the aforementioned CFD studies have applied the RANS (Reynolds-averaged Navier–Stokes) modelling method, while large-eddy simulation (LES) has been found to outperform RANS within real urban topographies including vegetation (Gousseau et al., 2011; Salim et al., 2011; Tominaga and Stathopoulos, 2011). Also, many of the previous studies on the effect of vegetation on pollutant ventilation and pedestrian-level air quality have been limited to idealised street canyons (Gromke and Ruck, 2012; Gromke et al., 2016; Moradpour et al., 2017; Santiago et al., 2017b; Vos et al., 2013; Vranckx et al., 2015). Furthermore, majority of the studies have treated passive pollutants but in order to take into account the aerosol dry deposition on vegetation, a description of the aerosol size distributions and dynamic processes need to be incorporated into modelling. Detailed treatment of aerosol processes is also needed when the behaviour of aerosol number concentrations, controlled by the most harmful ultrafine particles (UFP, Nel et al., 2006), is examined. To our knowledge, currently only two LES models, CTAG (Wang and Zhang, 2012; Wang et al., 2013; Tong et al., 2016) and PALM (Kurppa et al., 2019; Maronga et al., 2019), are able to account for the aerosol dynamics in simulating urban aerosol particle concentrations.

In this study, the contradictory effects of urban street trees on the pedestrian-level aerosol particle concentrations are examined using the LES model PALM (Maronga et al., 2015), which allows for a description of permeable vegetation and aerosol dynamics with dry deposition (Kurppa et al., 2019). The aim is to understand which of the studied and yet realistic street-tree layout scenarios minimise the pedestrian-level aerosol mass $PM_{2.5}$ and PM_{10} (particulate matter ≤ 2.5 μm and ≤ 10 μm, respectively) and number concentrations over the pavements and maximise aerosol particle ventilation within a boulevard-type street canyon with high traffic rates. Both combustion and vehicular suspension of road dust and two wind directions during a morning rush hour in late spring are considered. The research aim originated from the needs of urban planners in Helsinki as City of Helsinki is planning to convert its current motorway-like entry routes and their surroundings into a city boulevards surrounded with more densely built neighbourhoods (City of Helsinki, 2016). Thus, the focus is on the near future, i.e., year 2030.

2. Materials and methods

2.1. LES model

This study applies the PALM model system (version 6.0, revision 3698, Maronga et al., 2019), which features an LES core for atmospheric and oceanic boundary layer flows, and solves the non-hydrostatic, filtered, incompressible Navier–Stokes equations of wind (u, v, and w) and scalar variables (sub-grid scale (SGS) turbulent kinetic energy (TKE) e, potential temperature θ, and specific humidity q) in Boussinesq-approximated form. PALM is excellently scalable on massively parallel computer architectures (up to 50,000 cores, Maronga et al., 2015) and is therefore adapted for simulation domains up to the city-scale with a fine-enough grid resolution for building-resolving LES (Xie and Castro, 2006). Due to its specific features such as Cartesian topography scheme, plant canopy module and recently developed PALM-4U (short for PALM for urban applications) components, PALM is especially suitable for urban applications. Moreover, PALM includes a self-nesting capability to enable a fine grid resolution within the main domain of interest while having a large enough modelling domain and not exceeding the available computational resources (Maronga et al., 2019).

2.1.1. Canopy model

The aerodynamic effect of vegetation on flow is taken into account by an embedded canopy model. Vegetation decelerates the flow by

acting as a momentum sink, the magnitude of which depends on the wind velocity, leaf area density (LAD, $m^2\ m^{-3}$) and the aerodynamic drag coefficient C_D following:

$$\frac{\partial u_i}{\partial t} = \ldots - C_D \mathrm{LAD} \sqrt{u_i^2} u_i, \quad (1)$$

where u_i represents the wind components ($u_1 = u$, $u_2 = v$, $u_3 = w$). Furthermore, the effect on the SGS-TKE (e) is considered with an additional sink term in its prognostic equations:

$$\frac{\partial e}{\partial t} = \ldots - 2 C_D \mathrm{LAD} \sqrt{u_i^2} e. \quad (2)$$

LAD is defined as the total one-sided leaf area per unit volume and C_D quantifies the form and viscous drag forces caused by on obstacle to a fluid. Here a constant aerodynamic drag coefficient of 0.5 is used (Auvinen et al., 2020). This value is higher than more traditionally used 0.2, which has been found to be optimal for continuous plant canopies (Katul et al., 2004). For individual trees the value for C_D should be higher (Mayhead, 1973; Vollsinger et al., 2005). The canopy model itself was originally developed for continuous vegetation also, but has since been used for individual trees (e.g., Giometto et al., 2017). Recently a heterogeneous distribution of the tree canopy has been enabled in the model allowing to set up different LAD profiles for different grid points within the study area (Kurppa et al., 2018).

2.1.2. Aerosol module

To consider the dry deposition of aerosol particles on solid surfaces and vegetation, we apply the sectional aerosol module SALSA (Kokkola et al., 2008), which is part of the PALM-4U components (Kurppa et al., 2019). SALSA describes the aerosol number size distribution by a discrete number of size bins with a specific chemical composition, and comprises the aerosol processes of nucleation, condensation, dissolutional growth, coagulation and dry deposition on solid surfaces and vegetation. The advection and diffusion of aerosol number and mass are solved in the Eulerian framework.

Dry deposition on vegetation produces a sink term in the prognostic equations of concentrations

$$\frac{\partial N_i}{\partial t} = \ldots - \mathrm{LAD} v_{d,i} N_{i,t-\Delta t}, \quad (3)$$

where N_i is the aerosol number concentration in size bin i and $v_{d,i}$ is the dry deposition velocity, which can be solved using the parametrisation either by Zhang et al. (2001) or Petroff and Zhang (2010). On solid surfaces, dry deposition is implemented by means of a surface flux:

$$F_{N_i} = v_{d,i} N_{i,t-\Delta t}. \quad (4)$$

The same equations apply for mass concentrations $m_{c,i}$, where c is the chemical component.

2.1.3. PALM model evaluation

PALM cannot be evaluated against observations in this study as we simulate future scenarios. However, the different model parts have been successfully evaluated by previous studies. The performance of PALM has been evaluated against wind tunnel simulations over urban-like surfaces showing a good agreement for the mean flow and turbulence (Gronemeier and Sühring, 2019; Letzel et al., 2008; Razak et al., 2013), and scalar dispersion (Park et al., 2012) within the urban canopy and above. Only Gronemeier and Sühring (2019) reported slightly weaker re-circulation flow and turbulent fluctuations within a courtyard compared to a wind tunnel study by Hall et al. (1999). The plant canopy model has been successfully evaluated against a wind tunnel experiment downstream of a homogeneous forest patch (Kanani et al., 2014), showing that the plant canopy model in PALM adequately accounts for the drag of vegetation on the turbulent flow. Kurppa et al. (2019) evaluated the aerosol module against measured vertical profile of aerosol number concentration and size distribution in a simple street canyon in Cambridge, UK, and showed that the simulated values were mainly within a factor of two of the observations.

Correct initialisation and model boundary conditions are important for appropriate model simulation (Auvinen et al., 2020). In the present study, uncertainty resulting from these is minimised due to the comparative nature of the study with the different tree layout scenarios using the same initialisation and boundary conditions.

2.2. Modelled tree-layout scenarios and input data

The simulations are performed for a realistic city boulevard and its generalised surrounding neighbourhood (Fig. 1). Five street-tree layout scenarios (S1–S3) in addition to a baseline scenario without any trees (S0) are studied (Table 1 and Fig. 2). In scenarios S0, S2A, S2B and S2C the boulevard is 54 m wide, while it is 4 m wider in S1 and 4 m narrower in S3. The scenarios were decided together with local urban planners and the different street widths are suitable for each of the street-tree layout varying from two to four rows of trees. In all scenarios, there are in total eight traffic lanes. Tram lines are located in the middle and cycle lanes and pavements on both sides of the boulevard. As a default, the street trees are 15-m-tall *Tilia* × *vulgaris* (deciduous) trees, but in S2C the outermost trees are 9-m-tall *Sorbus intermedia* (deciduous). In S2B with three rows of trees, uniform hedges of 1 m in width and 0.75 m in height are set below the canopies of the outermost trees. In addition to the boulevard, some *Tilia* × *vulgaris* trees are also added to the surroundings (see Fig. 1).

The city blocks along the boulevard are manually constructed into a three-dimensional model based on a development plan of the City of Helsinki (personal communication 2.7.2018). The boulevard is surrounded by generic cuboids that generate appropriate aerodynamic roughness of the surrounding urban area with detached houses. Specifically, a 64 m × 64 m tile containing four generic cuboids is repeated. Morphological details of the buildings are given in Table 2. Land surface elevation is neglected and a flat terrain is applied everywhere.

2.2.1. Vegetation

The three-dimensional shape of street trees is formed from airborne laser scanning (ALS) tree inventory of urban roadside trees in the City of Helsinki (Tanhuanpää et al., 2014). First, the inventory is filtered by the used tree species (i.e., *Tilia* × *vulgaris* and *Sorbus intermedia*) and then by

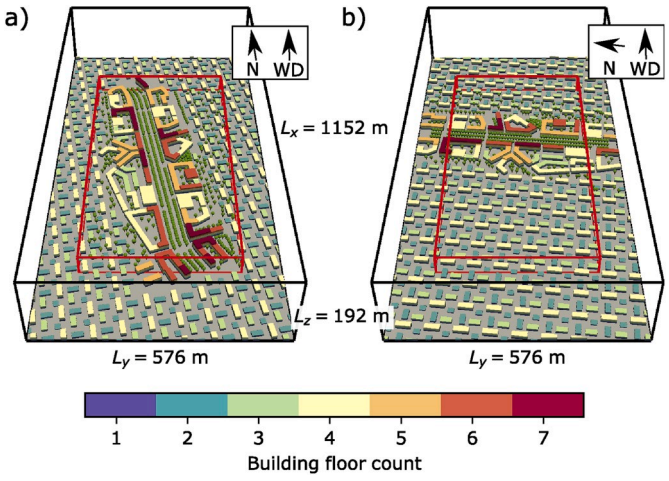

Fig. 1. Modelling domains with wind direction a) parallel (WD = 8°) and b) perpendicular (WD = 82°) to the boulevard. The floor height equals 3 m. The boundaries of the parent domain are shown in black and those of the child domain in red. L_x, L_z and L_z indicate the dimensions of the parent domain in x-, y- and z-directions and N north. (For interpretation of the references to colour in this figure legend, the reader is referred to the Web version of this article.)

Table 1
Planning scenarios investigated in this study. All *Tilia* × *vulgaris* trees are 15 m and *Sorbus intermedia* 9-m-tall. CVF stands for crown volume fraction, i.e., volume of total tree crown divided by the average street canyon volume.

Scenario	Boulevard width (m)	Rows of trees	Tree species	Hedges	CVF
S0	54	0	–	–	0.00
S1	58	4	*Tilia* × *vulgaris*	–	0.19
S2A	54	3	*Tilia* × *vulgaris*	–	0.16
S2B	54	3	*Tilia* × *vulgaris*	Below outermost trees	0.16
S2C	54	3	*Tilia* × *vulgaris* (middle), *Sorbus intermedia* (outermost)	–	0.09
S3	50	2	*Tilia* × *vulgaris*	–	0.11

an appropriate tree height (14–16 m and 9–10 m, respectively). This yields 819 matches for *Tilia* × *vulgaris* and 87 matches for *Sorbus intermedia*. Dimensionless vertical profiles are then calculated based on the average pulse return height distribution of the filtered trees. A mean value for the maximum horizontal diameter of the tree crown is calculated for both species. Then, three-dimensional circularly symmetric shape masks of the tree crowns are constructed so that their diameter and horizontally integrated profile match the ones from the ALS data (Fig. 3 and S1 in the Supplement). For all masked points, a conservative estimate LAD = 1.2 m^2 m^{-3} for broad-leaved trees is used (Abhijith et al., 2017). For hegdes LAD = 2.0 m^2 m^{-3} (Wania et al., 2012). All model simulations are made in late spring and thus LAD values correspond to summertime values.

2.2.2. Aerosol particle boundary conditions

Traffic-related emissions are treated as area sources from the eight 3-m-wide traffic lanes (Fig. 2) occupying 41–48% of the boulevard surface area. Six lanes are located on the main street along the boulevard and two on the smaller streets at the side. The applied traffic rate 3660 veh h^{-1} is an estimate for a typical morning rush hour on a boulevard-type entry route in Helsinki and the traffic is equally distributed on all lanes. The fleet composition (81% passenger cars, 10% light and 3% heavy duty diesel vehicles, and 6% buses) is estimated from present-day traffic counts in Helsinki. The distribution of different vehicle technologies (diesel, fuel, electric) is based on ALIISA model estimation for year 2030 (VTT, 2018) with the difference that 30% of the bus fleet is assumed to be electric according to the rolling stock scenario of the local public transportation in Helsinki for 2030.

The unit emissions of combustion-related $PM_{2.5}$ (g m^{-1} veh^{-1}) for year 2030 are drawn from the LIPASTO unit emission database (VTT, 2018). For vehicle suspension of road dust, a unit emission of 315 μg m^{-1} veh^{-1} is estimated using the FORE road dust model (Kauhaniemi et al., 2011). This value is the 75-percentile for dry and medium-windy morning rush hours (7–9 am) in April–May 2007–2009 and 2014. To select only these meteorological conditions, hours with non-zero accumulated precipitation and hourly mean horizontal wind

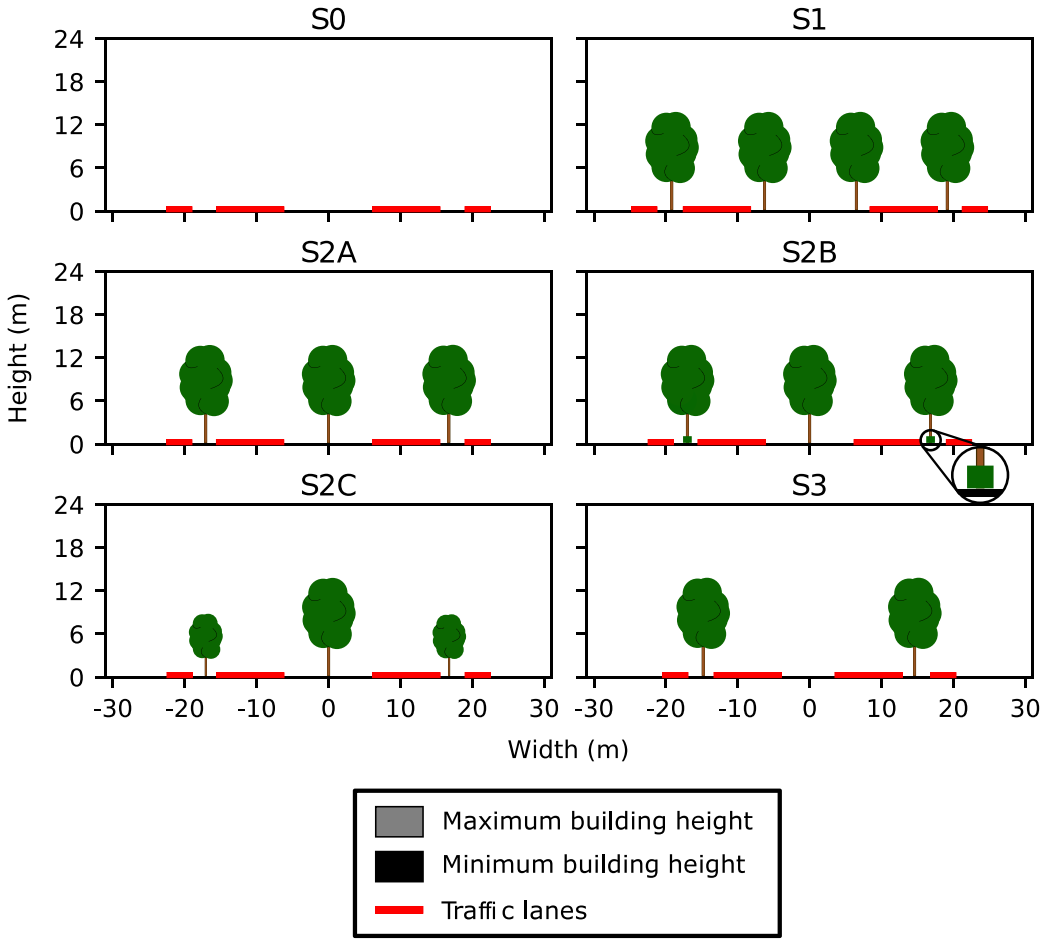

Fig. 2. Cross section for the street-tree layout scenarios. One of the hedge rows is highlighted for S2B. See Table 1 for details.

Table 2
Morphometric properties of buildings in different modelling domains for both wind directions (WD = 8° and WD = 82°). $H_{b,avg}$ is the area-weighted average, $H_{b,min}$ is the minimum and $H_{b,max}$ is the maximum building height. λ_p is the plan area fraction (i.e., fraction of the building plan area to the total plan area) and λ_f is the frontal aspect ratio (i.e., ratio of the building facade area in the direction of the mean wind to the total plan area).

Area	$H_{b,avg}$ (m)	$H_{b,min}$ (m)	$H_{b,max}$ (m)	λ_p	λ_f
Full domain (WD = 8°)	10.3	4.0	21	0.34	0.19
Full domain (WD = 82°)	9.6	4.0	21	0.35	0.23
Nested child domain (WD = 8°)	12.7	4.0	21	0.33	0.20
Nested child domain (WD = 82°)	10.4	4.0	21	0.35	0.23
Along the boulevard	17.2	12.0	21.0	–	–
Surrounding urban area ((WD = 8°)	8.2	4.0	12.0	0.36	0.18
Surrounding urban area (WD = 82°)	8.2	4.0	12.0	0.36	0.23

speed below 3.3 m s^{-1} or over 6.3 m s^{-1} were filtered out based on observations at the Kaisaniemi meteorological station in Helsinki at z = 32 m (Finnish Meteorological Institute, 0000). Finally, for the specific fleet composition, traffic rate and total lane width of 8 × 3 m, traffic emission factors$EF_{PM_{2.5}} = 3.18 \times 10^{-7}$ g m^{-2} s^{-1} and $EF_{PM_{10}} = 1.69 \times 10^{-5}$ g m^{-2} s^{-1} are obtained.

The background concentrations $PM_{2.5} = 5.42$ μg m^{-3} ($\sigma_{PM_{2.5}} = 3.42$ μg m^{-3}, $\min(PM_{2.5}) = 2.10$ μg m^{-3}, $\max(PM_{2.5}) = 19.50$ μg m^{-3}) and $PM_{10} = 17.37$ μg m^{-3} ($\sigma_{PM_{10}} = 11.52$ μg m^{-3}, $\min(PM_{10}) = 6.00$ μg m^{-3}, $\max(PM_{10}) = 61.20$ μg m^{-3}) represent the mean values for morning (7–9 am) rush-hours at an urban background station located in Helsinki between April–June 2008–2018. Similar to the road dust emissions, only dry and medium-windy meteorological conditions are considered.

The aerosol emissions and background concentrations are given to SALSA as aerosol number. Mass emissions are translated to number emissions by assuming the following tri-modal log-normal aerosol size distribution: nuclei mode (geometric number mean diameter $\overline{D}_{g,n}$ = 11.7 nm and mode standard deviation $\sigma_n = 1.71$) particles represent 1% and Aitken mode ($\overline{D}_{g,a} = 37.3$ nm and $\sigma_a = 1.78$) particles 99% of $EF_{PM_{2.5}}$, while coarse mode ($\overline{D}_{g,c} = 864$ nm and $\sigma_c = 2.21$) particles represent the whole $EF_{PM_{10-2.5}} = EF_{PM_{10}} - EF_{PM_{2.5}}$. The background aerosol size distribution is assumed to follow the polluted urban type size distribution applied in Zhang et al. (1999) so that nuclei mode particles represent 1.6% and accumulation mode 98.4% of $PM_{2.5}$, while coarse mode particles represent the whole $PM_{10-2.5}$. The sectional representation of the size distributions is shown in Fig. S3.

2.3. Simulation setup

All simulations are conducted over a domain of 384 × 192 × 64 in x-, y- and z-directions with a uniform grid resolution of 3 m. Within, a nested child domain of 768 × 384 × 72 with a grid resolution of 1.0 m in horizontal and 0.75 m in vertical is defined (Fig. 1). For a typical urban street network in Helsinki, this spatial resolution has been found sufficient to solve the flow in the vicinity of urban roughness elements and close to the ground (Auvinen et al., 2020). This also meets the grid spacing requirement suggested by Xie and Castro (2006) as the smallest buildings of 12 m in height along the boulevard are resolved using 16 grid points (Table 2). For all scenarios, neutral atmospheric stratification and two different wind directions relative to the boulevard, WD = 8° (hereafter parallel) and WD = 82° (hereafter perpendicular), are considered. The morphometric properties of the simulation domain for both wind directions are represented in Table 2.

Due to the high computational demands of SALSA, and especially that of resolving advection for a large number of aerosol number and mass bins (Kurppa et al., 2019), the aerosol module is applied only within the nested domain. The aerosol size distribution is modelled for a size range 3 nm–10 μ m using ten size bins (see Table S1). Dry deposition does not depend on the aerosol chemical composition, and therefore only solid aerosol particles containing organic carbon are considered. Aerosol size-specific dry deposition velocities are calculated every $\Delta t_{SALSA} = 1.0$ s by Zhang et al. (2001) using the land use category "deciduous broadleaf trees" for vegetation and "urban" for buildings. The values range between $v_d \sim 1$ cm s^{-1} for the smallest particles and $v_d \sim 0.01$ cm s^{-1} for particles of around 500 nm in diameter. To simulate constant background concentrations, aerosol concentrations are fixed at the lateral and top boundaries.

For the wind, specific humidity (q) and SGS-TKE (e), cyclic boundary conditions are applied at the spanwise boundaries while non-cyclic conditions are set at the streamwise boundaries. The mean part of the streamwise boundary conditions are obtained from a precursor run. The precursor run is conducted over a domain equal in size with the full domain and run with cyclic lateral boundary conditions for T = 6 h to create a quasi-stationary flow field. Surface roughness equal to the idealised generic roughness elements (Table 2) is introduced at the bottom to create and maintain turbulence in the precursor run. The precursor wind field is driven with a uniform pressure gradient of $\frac{\partial p}{\partial x} = -1.499 \times 10^{-3}$ Pa m^{-1} and $\frac{\partial p}{\partial y} = -5.235 \times 10^{-5}$ Pa m^{-1} (Fig. S2). In addition to the mean part, turbulence recycling method is used to add to the mean streamwise boundary conditions. A recycling plane is placed downstream the focus area, with turbulence being recycled back from the plane to the inbound boundary. Slightly slanted (2°) wind directions relative to the domain were used in order to avoid persistent spanwise locking of large-scale turbulent structures (Munters et al., 2016). For the nested domain, one-way nesting to the parent domain is used to obtain the flow boundary conditions.

At top boundary, Neumann (zero-flux) condition is set for wind and scalars, while at bottom Dirichlet (fixed boundary) condition is set for wind and Neumann for scalars. Furthermore, at all solid walls, Monin-Obukhov similarity theory with the roughness length $z_0 = 0.03$ m is applied. The advection of momentum and scalars variables is based on the 5th-order advection scheme by Wicker and Skamarock (2002) together with a third-order Runge-Kutta time stepping scheme (Williamson, 1980). The pressure term in the prognostic equations for momentum is calculated using the iterative multigrid scheme (Hackbusch, 1985).

All simulations are first run for T = 600 s after which data output is collected for the following T = 1 h. Simulations are performed on Cray XC40-based Sisu supercomputer of the CSC - IT Center for Science, Finland, using 4 × 2 and 24 × 12 Intel Xeon E5-2690v3 Haswell microarchitecture processor cores for the full and child domain, respectively. Each simulation uses approximately 1000 days of CPU time.

2.4. Data analysis

Both time series and temporally averaged data are collected from simulations. In this study, the focus is only on the child domain. Data analysis is conducted far enough from the lateral boundaries of the child domain to minimise the impact of concentration discontinuity due to the fixed aerosol boundary conditions on the lateral and top boundaries.

Firstly, 1-min averaged values of PM_{10}, $PM_{2.5}$, total aerosol number concentration (N_{tot}) and wind components are saved at each vertical level between $z = 0.4 - 32$ m. $PM_{2.5}$, PM_{10} and N_{tot} are calculated within PALM as the total aerosol mass of particle $\overline{D}_g < 2.5$ μm and $\overline{D}_g < 10$ μm, and number, respectively. Secondly, aerosol size distributions are saved every 2 s and wind components every second at four levels between $z = 1.9 - 23.6$ m. All wind components are interpolated

to the same grid points as scalar variables, that is in the middle of each model grid cell.

The concentrations on the pavements are specifically defined at 3 m from the wall along 250-m-long lines on both sides of the boulevard. Concentrations over pavements and the whole boulevard are analysed at $z = 1.9$ m above ground (referred as pedestrian-level) which corresponds to the approximated inhaling height. The term pavement is used to refer to pedestrian areas on the side of streets which in American English would be referred to as sidewalks.

To represent the magnitude of the mean circulation within the street canyon, a volumetric flow rate across the street canyon per unit length Q is calculated for the perpendicular wind direction (WD = 82°). The mean circulation is defined from the stream function averaged along the boulevard

$$\Psi(x_r,\ z) = \frac{1}{y_{r,2} - y_{r,1}} \int_0^z \int_{y_{r,1}}^{y_{r,2}} \overline{u_r}\ (x_r,\ y_r,\ z)\ dy_r\ dz, \tag{5}$$

in rotated coordinates so that x_r-axis is perpendicular and y_r-axis is parallel to the boulevard, z is the height above ground, $\overline{u_r}$ is the mean of wind component u_r perpendicular to the boulevard and $(y_{r,1}, y_{r,2})$ covers a 250-m-long section of the boulevard. Then, Q is specified as the absolute value of the stream function's minimum in the $(x_r,\ z)$ -plane.

Vertical turbulent flux F measures pollutant ventilation due to turbulent transport. In this study, F is calculated only for the aerosol size bin 6 ($\overline{D}_g$ = 303.3 nm) because this size range has the lowest deposition velocity (Kurppa et al., 2019) and is thus least affected by dry deposition. Hence, F_{bin6} is the covariance between w and aerosol number concentration N

$$F_{bin6} = \overline{w' N_{bin6}'}\ , \tag{6}$$

where $w'(t,x,y,z)$ and $N'_{bin6}(t,x,y,z)$ are the instantaneous fluctuating values at point (x,y,z) at time t, and the overbar denotes the time average (here 1 h). Positive F_{bin6} indicates upward transport, i.e., ventilation. Furthermore, data to calculate F_{bin6} have a temporal resolution of Δt_{flux} = 2 s. Hence, we acknowledge that the contribution of eddies with time scales smaller than Δt_{flux} is ignored here.

The mean (MKE) and turbulent kinetic energy (TKE) of the flow at tree heights ($z = 1.9 - 14.6$ m) were studied independently. MKE was calculated as

$$MKE = \frac{1}{2}\left(\overline{u}^2 + \overline{v}^2 + \overline{w}^2\right)\ , \tag{7}$$

where $\overline{u}$, $\overline{v}$ and $\overline{w}$ are the 1-h averaged wind components in (x,y,z) direction, and TKE as

$$TKE = \frac{1}{2}\left(\overline{(u')^2} + \overline{(v')^2} + \overline{(w')^2}\right)\ , \tag{8}$$

where $\overline{(u')^2}$, $\overline{(v')^2}$ and $\overline{(w')^2}$ are the 1-h averaged variances of the wind components.

3. Results

The very detailed spatial variability of the pedestrian-level N_{tot} and PM_{10} within the study domain is demonstrated in Fig. 4. The highest concentrations with clear hot spots are observed near the source on the boulevard and the concentrations rapidly decrease when moving away on the side streets and courtyards. In this study, both aerosol mass ($PM_{2.5}$ and PM_{10}) and number concentrations are examined, and as $PM_{2.5}$ behaves very similarly to PM_{10}, figures for $PM_{2.5}$ are shown only in the Supplement. A special focus is on the pavements on both sides of the boulevard, which is assigned accordingly in the figures, while mean values over the whole boulevard are denoted with angular brackets ⟨…⟩ hereafter.

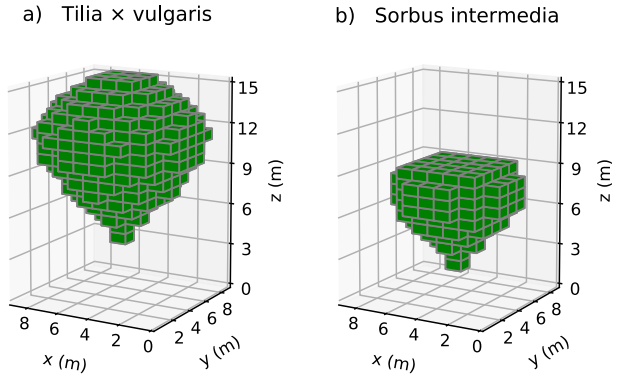

Fig. 3. Three-dimensional models of a) *Tilia* × *vulgaris* and b) *Sorbus intermedia* trees used in the study. Cuboids show the placement of within-canopy grid points.

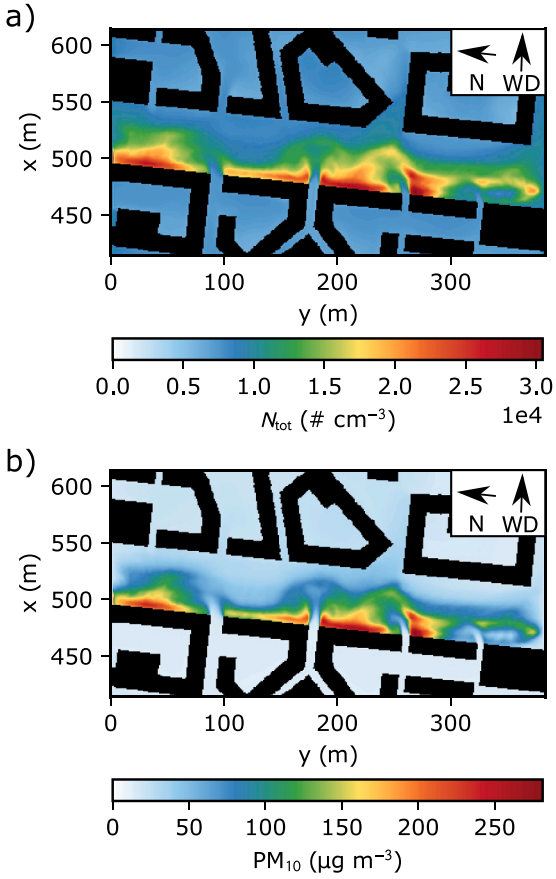

Fig. 4. The spatial variability of the pedestrian-level (z = 1.9 m) concentrations of a) N_{tot} and b) PM_{10} in the vicinity of the boulevard for the scenario S2A with parallel wind (WD = 82°). *N* indicates north.

3.1. Concentrations on pavements

The mean values and variation of PM_{10} and N_{tot} on the pavements on both sides of the boulevard are illustrated in Figs. 5 and 6, respectively (see Fig. S4 for $PM_{2.5}$). The lowest mass concentrations (PM_{10} mean values $28 - 75$ μg m^{-3} and $PM_{2.5}$ $9 - 16$ μg m^{-3}) and least variability are seen in the scenario S0 where there are no trees along the boulevard. Introducing vegetation along the boulevard increases aerosol mass with

both wind directions. Depending on the scenario and direction of the wind relative to the boulevard, planting trees increases the mean PM_{10} by 4–123% (Table 3) and $PM_{2.5}$ by 1–72% (Table 4). The scenario S2C with three rows of trees and smaller outermost trees shows least variation (excluding the western side with perpendicular wind) indicating lower peak concentrations when compared to the other scenarios. None of the scenarios show systematically lowest or highest concentrations. For example, on the eastern side with wind parallel to the boulevard, S2C shows the lowest (30%) and S1 the highest increase (73%) in PM_{10} concentrations, but on the western side with perpendicular wind, S2A creates the highest (123%) and S1 the smallest increase (107%). In general, the highest concentrations are seen on the western and lowest concentrations on the eastern side with perpendicular wind due to a canyon vortex that pushes pollutants to the western side.

If the relative differences of the mean and median values are calculated, S2C shows the lowest concentrations relative to the treeless case S0 and increases PM_{10} by 69% and $PM_{2.5}$ by 33% compared to >75% and >35%, respectively, in other scenarios. One should notice that besides the tree layout, the street widths are different in scenarios S0, S2A, S2B and S2C, S1 and S3 and thus the pure effect of trees can be revealed only by comparing the scenarios with the same street-canyon width (S0, S2A, S2B and S2C). The three rows of uniform trees in S2A create the highest mass concentrations on the pavements (+88% and +42% for PM_{10} and $PM_{2.5}$), yet the increase in concentrations is smaller when hedges are introduced below the tree canopies in S2B (+75% and +35% for PM_{10} and $PM_{2.5}$, respectively). The effect of trees is stronger on PM_{10} than on $PM_{2.5}$ concentrations. Slightly higher mass concentrations are observed in S3 (narrower) than in S1 (wider).

Distinct differences are seen in the effect of the different scenarios on aerosol mass and number. Similar to $PM_{10/2.5}$, the lowest N_{tot} are seen in

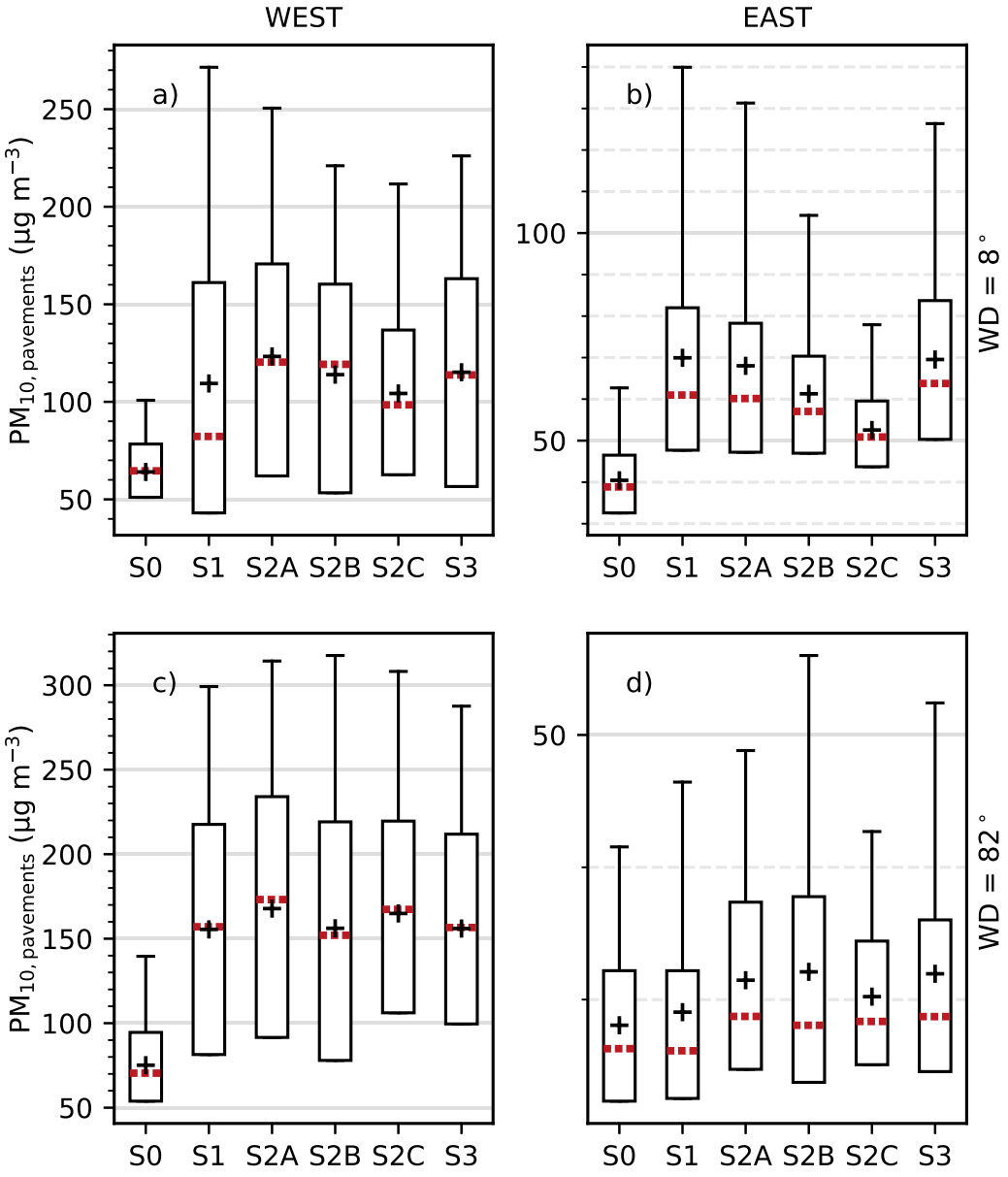

Fig. 5. Hourly PM_{10} concentrations (µg m^{-3}) at $z = 1.9$ m on the pavement on the western (a,c) and eastern (b,d) side of the boulevard with parallel (WD = 8°, a-b) and perpendicular (WD = 82°, c-d) wind. Black plus signs show mean values, red dashed lines medians, the lower and upper limit of the boxes 25th and 75th percentiles and whiskers the 95th percentiles. (For interpretation of the references to colour in this figure legend, the reader is referred to the Web version of this article.)

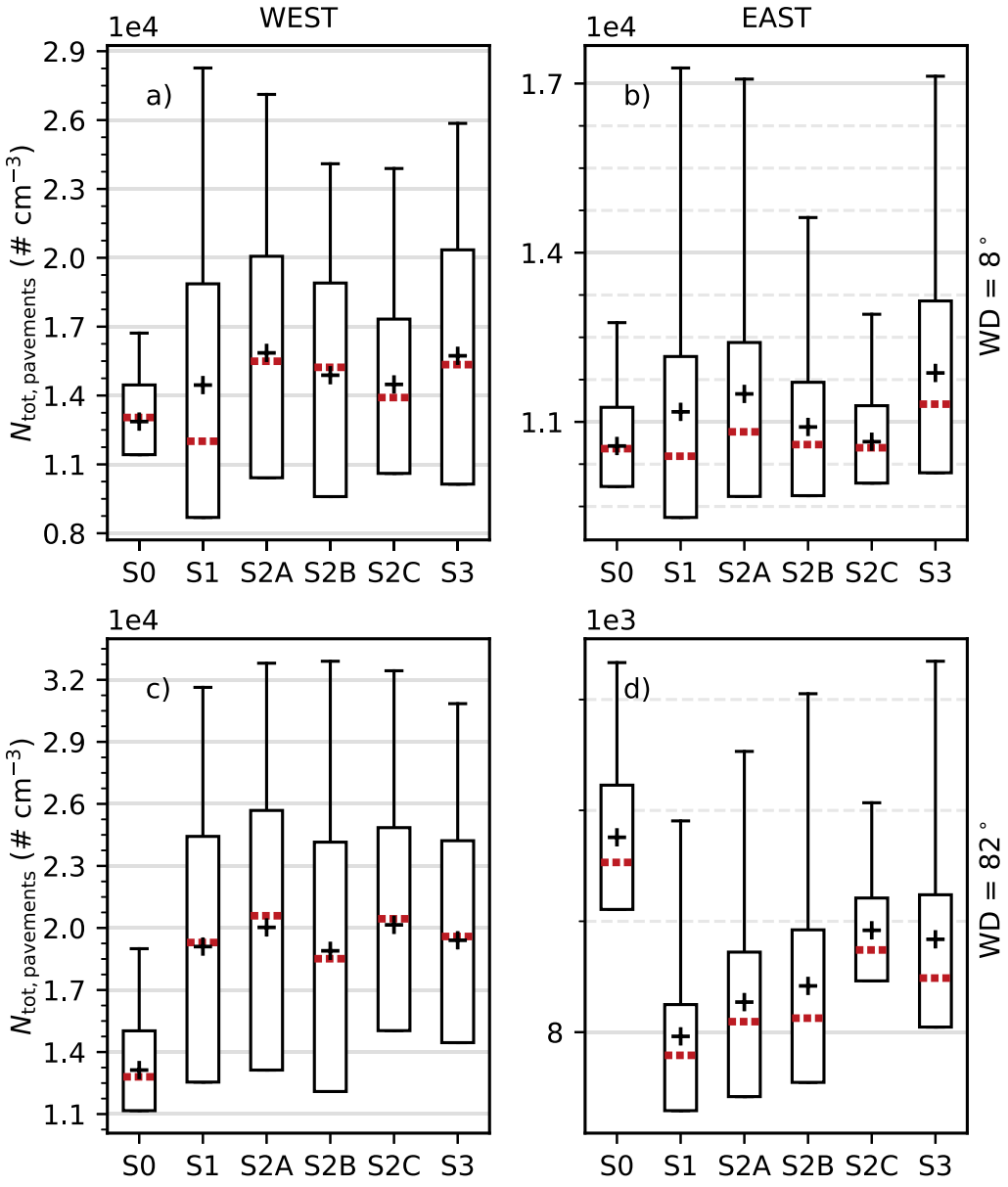

Fig. 6. Hourly total aerosol number concentrations N_{tot} (# cm^{-3}) at $z = 1.9$ m on the pavement on the western (a,c) and eastern (b,d) side of the boulevard with parallel (WD = 8°, a-b) and perpendicular (WD = 82°, c-d) wind. See Fig. 5 for details.

Table 3
Relative difference in mean (median in brackets) PM_{10} (%) concentrations on the pavements compared to baseline scenario S0 at $z = 1.9$ m.

WD	Side	S1	S2A	S2B	S2C	S3
Parallel (8°)	West	+71 (+27)	+92 (+86)	+78 (+85)	+63 (+52)	+80 (+76)
	East	+73 (+57)	+68 (+55)	+52 (+47)	+30 (+31)	+72 (+64)
Perpendicular (82°)	West	+107 (+123)	+123 (+146)	+108 (+116)	+119 (+138)	+108 (+122)
	East	+4 (−1)	+12 (+9)	+14 (+7)	+8 (+8)	+14 (+9)
Mean		+75 (+63)	+88 (+91)	+75 (+78)	+69 (+72)	+79 (+81)

Table 4
Relative difference in mean (median in brackets) $PM_{2.5}$ (%) concentrations on the pavements compared to baseline scenario S0 at $z = 1.9$ m.

WD	Side	S1	S2A	S2B	S2C	S3
Parallel (8°)	West	+30 (+7)	+44 (+40)	+35 (+39)	+28 (+23)	+40 (+37)
	East	+30 (+23)	+29 (+23)	+22 (+20)	+12 (+13)	+32 (+28)
Perpendicular (82°)	West	+63 (+72)	+72 (+85)	+62 (+66)	+71 (+81)	+64 (+72)
	East	+1 (−1)	+5 (+4)	+5 (+2)	+3 (+3)	+5 (+3)
Mean		+35 (+28)	+42 (+43)	+35 (+36)	+33 (+34)	+39 (+39)

the scenario without trees (S0). On the contrary, all scenarios with trees show a decrease in the mean number concentration up to 14% (Table 5) on the eastern side with perpendicular wind. Otherwise, trees increase the mean N_{tot} by 1–53%. Again, outside S0 less variance is seen in S2C than in other scenarios but the spread in the means and medians among the different scenarios is wider when compared to mass concentrations. As for aerosol mass, the largest concentrations are seen on the western side with wind perpendicular to the boulevard. Of all scenarios, S1 with four rows of trees and a wider street canyon performs best from the point of view of aerosol number concentrations and increases the mean concentrations by 15% relative to the treeless scenario S0 (other scenarios 16–21%). When looking the scenarios with same street canyon width (S0, S2A, S2B and S2C), the lowest N_{tot} is seen with hedges under the outermost trees (in S2B). Also the height variability of trees (in S2C) improves the number concentrations when compared to the three rows of uniform trees (in S2A). The influence of trees on aerosol number is much less (the maximum difference compared to the treeless scenario 53%) than those on aerosol mass (the maximum difference 120% for PM_{10} and 71% for $PM_{2.5}$).

The lowest concentrations observed in S0 are concurrent with, on average, the most effective vertical dispersion of aerosol particles (see vertical profiles in Fig. S5–S7). Similarly, the notably low values in S2C on the eastern side with perpendicular wind coincide with clearly more effective vertical dispersion (Fig. S5b, S6b and S7b). The relative differences in the vertical profiles between the scenarios are larger for N_{tot} than $PM_{2.5}$ and PM_{10}, which is consistent with the spread in the mean values and variation (Figs. 5 and 6 and S4).

To compare the street-tree scenarios without the impact of varying street widths, the relationship between the crown volume fraction (CVF, the total tree crown volume divided by that of the entire street canyon; Table 1) and the mean concentrations (PM_{10} and N_{tot}) on the pavements (Fig. 7) is examined. CVF varies from 0 to 0.19, with the smallest non-zero CVF in S2C with variable tree heights and the largest in S1 with four rows of trees and a slightly wider street canyon. Note that the difference in CVF between S2A with three rows of uniform trees and S2B with additional hedges is only minor. As shown also in Figs. 5–6 and Tables 3–5, concentrations on the pavements are increased when trees are introduced to the boulevard (S1–S3), while no systematic increase in concentrations with CVF can be observed when only S1–S3 are considered. However, for the concentrations averaged over the whole boulevard, a more evident linear relationship (see Fig. S8) between CVF and concentrations when the wind is parallel to the boulevard is revealed ($R^2 = 0.97$ and $R^2 = 0.96$ for PM_{10} and N_{tot}, respectively). With perpendicular wind, no clear dependence can be observed between CVF and concentrations, and N_{tot} is even shown to decrease with increasing CVF in S1–S3. This more complicated pattern with increasing CVF is due to the more effective dry deposition of small aerosol particles (dominating N_{tot}) to vegetation (see Section 3.2).

Table 5
Relative difference in mean (median in brackets) N_{tot} (%) concentrations on the pavements compared to baseline scenario S0 at $z = 1.9$ m.

WD	Side	S1	S2A	S2B	S2C	S3
Parallel (8°)	West	+12 (−8)	+23 (+19)	+16 (+17)	+13 (+7)	+22 (+18)
	East	+6 (−1)	+9 (+3)	+3 (+1)	+1 (±0)	+12 (+7)
Perpendicular (82°)	West	+45 (+51)	+53 (+61)	+44 (+45)	+53 (+60)	+48 (+53)
	East	−14 (−14)	−12 (−12)	−11 (−12)	−7 (−6)	−7 (−9)
Mean		+15 (+9)	+21 (+21)	+16 (+15)	+18 (+17)	+21 (+20)

3.2. Impact on aerosol size distribution

Fig. 8 illustrates the relative difference in the mean aerosol size distribution for the scenarios with trees (S1–S3) compared to the baseline scenario S0. Size distributions are calculated over the whole boulevard at four heights and for both wind directions. In general, introducing street trees leads to up to 50% lower number concentrations $\langle N \rangle$ for the smallest size bins (diameter $\overline{D}_g = 4.8$ nm and $\overline{D}_g = 12.5$ nm) over the whole boulevard, whereas aerosol particles in the size ranges $50 < \overline{D}_g < 500$ nm and $\overline{D}_g > 1$ μm show a clear increase up to 30% and 100% compared to S0, respectively. Furthermore, very minor differences are observed in the size range 500 nm $< \overline{D}_g < 1$ μm. The impact of trees is quickly attenuated above the roof level ($z = 23.6$ m). The relative differences in aerosol size distributions can be explained as a sum of different deposition velocities and size distributions of aerosol emissions: deposition velocities are largest for the smallest particles and smallest for particles around $\overline{D}_g = 500$ nm (Kurppa et al., 2019), and aerosol emissions, compared to the background concentrations, largest for size ranges 10 nm $< \overline{D}_g < 100$ nm and $\overline{D}_g > 800$ nm (see Fig. S3).

With parallel wind, S2C shows the smallest and S1 the largest differences compared to S0, while with perpendicular wind $|\Delta\langle N \rangle|$ is generally the smallest in S1. Especially for aerosol particles $\overline{D}_g > 1\ \mu m$, $\Delta\langle N \rangle$ are higher for the parallel than the perpendicular wind direction. Interestingly, $\langle N \rangle$ for this size range is still noticeable higher above the mean building height when the wind is parallel to the boulevard (Fig. 8g). This is observed both for the upwind and downwind part of the boulevard (see Fig. S9).

Comparing CVF and $\Delta\langle N \rangle$ for different aerosol size ranges over the whole boulevard shows that for UFP ($\overline{D}_g < 100$ nm), $\Delta\langle N \rangle$ decreases with increasing CVF with no systematic difference in wind directions (down to −20%, see Fig. S10) as also seen in Fig. 8. Larger particles, instead, show a systematic increase with CVF, with higher $\Delta\langle N \rangle$ values with parallel wind (up to 65%).

3.3. Pollutant ventilation

The ventilation (or vertical dispersion) of aerosol particles by both the turbulent and mean flow is assessed investigating the vertical turbulent flux (F_{bin6}), the volumetric flow rate across the street canyon per unit length (Q) with perpendicular wind, and also the mean (MKE) and turbulent kinetic energy (TKE).

The mean values and variation of vertical turbulent exchange $\langle F_{bin6} \rangle$ (see Eq. (6)) over the whole boulevard at two heights are shown in Fig. 9 and Table 6. The lower level ($z = 14.6$ m) is located near the crown top of *Tilia* × *vulgaris* trees (Fig. 3) and the upper level ($z = 23.6$ m) around 3 m above the highest buildings (Table 2). With parallel wind (Fig. 9a and c), introducing trees to the boulevard increases $\langle F_{bin6} \rangle$ at both levels by 13–70%. On average, $\langle F_{bin6} \rangle$ is highest in S2C (mean 1.1×10^6 m^{-2} s^{-1}), in which the flux variation is also lowest. At the lower level, the differences between S2A and S2B with additional hedges are very minor (mean increase 38% and 37%), while above buildings higher values are observed in S2A (mean increase 38% and 30%, respectively). $\langle F_{bin6} \rangle$ is shown to decrease upwards, but still above the roof level the influence of trees and tree layouts is evident with 15–48% higher $\langle F_{bin6} \rangle$ in the scenarios with trees. Due to wind sweeping pollutants from the southern to the northern end of the boulevard, concentrations and hence also fluxes are slightly higher in the northern end (not shown).

With perpendicular wind (Fig. 9b and d), $\langle F_{bin6} \rangle$ at the lower level is clearly highest in S0 without trees (mean 6.3×10^5 m^{-2} s^{-1}) and lowest in S1 with four rows of trees (−65%). Thus, trees disturb the vertical turbulent transport from the boulevard with perpendicular wind. Actually, the 25-percentile of $\langle F_{bin6} \rangle$ is even negative for S1, S2A and S2B indicating entrainment of more polluted air to the street canyon on the eastern side of the boulevard (not shown). However, above rooftop the

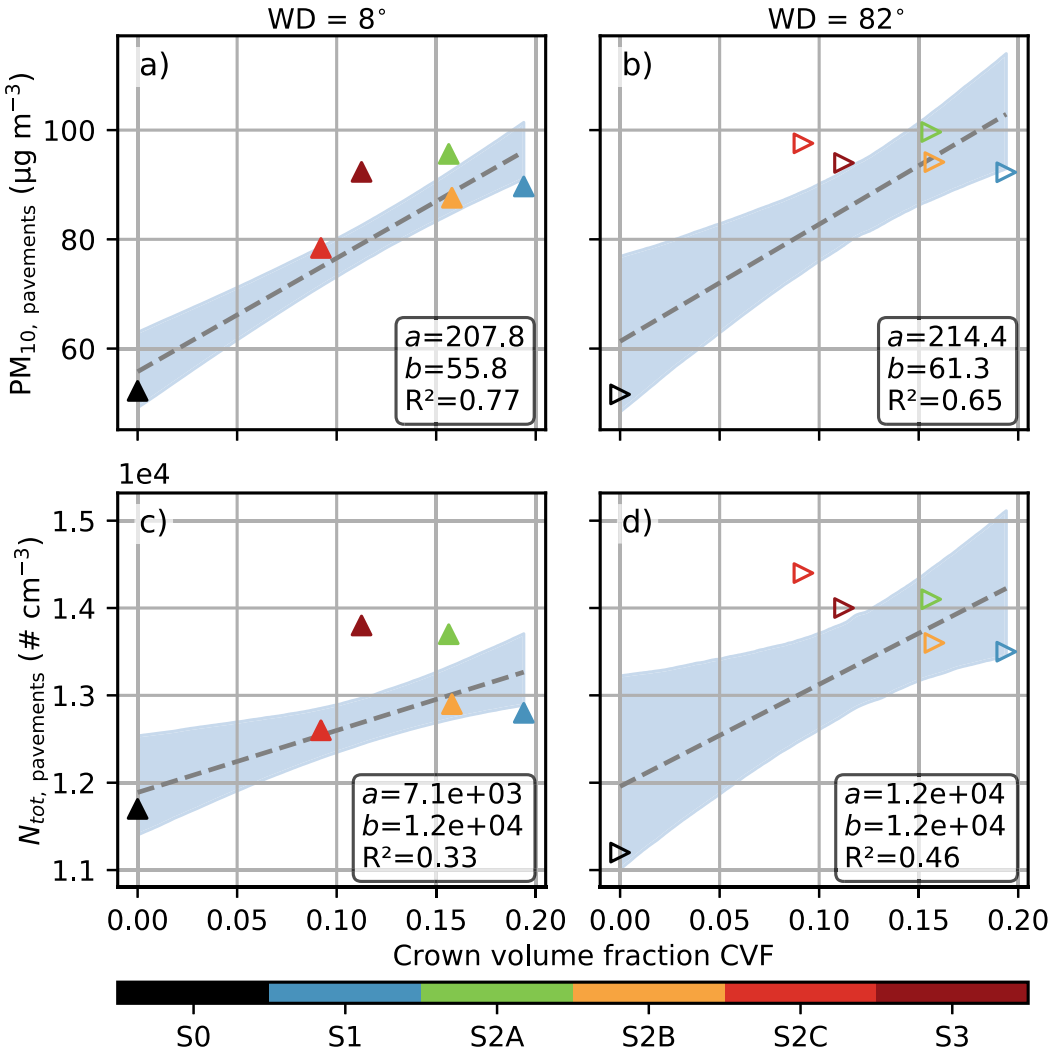

Fig. 7. The relationship between the crown volume fraction (CVF) over the whole boulevard and the mean PM_{10} (a,b) and N_{tot} (c,d) concentrations on the pavements in different scenarios with parallel (WD = 8°, left column: a, c) and perpendicular (WD = 82°, right column: b, d) wind. The grey dashed lines are linear least squares fits and the blue shaded areas represent the 95% confidence intervals of the fitted lines obtained using the bootstrap method using 10,000 bootstrap samples. (For interpretation of the references to colour in this figure legend, the reader is referred to the Web version of this article.)

hourly averaged fluxes become very uniform and the impact of trees on the average fluxes nearly disappears. Only difference is the slightly lower variation in S1 and S2C.

For the mean flow transport of aerosols, Fig. 10 shows the pedestrian-level a) $\langle PM_{10} \rangle$ and b) $\langle N_{tot} \rangle$ as a function of Q only with perpendicular wind. Q, representing the magnitude of the mean circulation, is the largest (5.6 mm^2 s^{-1}) when there are no trees in the street canyon (S0) and the smallest (4.3 mm^2 s^{-1}) in S2A with three rows of trees. Of all scenarios with trees, S2C has the largest Q. Both concentrations decrease with increasing Q showing how the mean flow effectively transports aerosol particles away from the boulevard. The relationship is stronger for PM_{10} with $R^2 = 0.66$, while no clear correlation can be observed between Q and N_{tot} ($R^2 = 0.18$). Hence, for N_{tot} other processes than the magnitude of the average circulation are also important. This agrees with the findings in Section 3.2, which shows how the dry deposition is more effective for the smaller particle size ranges.

To further assess the relationship of the mean flow and turbulence with ventilation, pedestrian-level $\langle PM_{10} \rangle$ is analysed as function of $\langle$MKE$\rangle$ and $\langle$TKE$\rangle$ at several heights (Figs. 11 and 12). Generally, larger $\langle$MKE$\rangle$ values are observed with wind parallel to the boulevard than with perpendicular wind. Also, the mean $\langle$MKE$\rangle$ within the street canyon is clearly largest in S0, which can be expected as trees act as momentum sinks. With parallel wind, the pedestrian-level $\langle PM_{10} \rangle$ shows negative linear relationship with $\langle$MKE$\rangle$, especially with $\langle MKE \rangle_{14.6\ m}$. Instead, no linear relationship between $\langle$MKE$\rangle$ and $\langle PM_{10} \rangle$ can be observed with perpendicular wind and all scenarios with trees show nearly equal $\langle$MKE$\rangle$ values. But as shown above, increasing Q, which specifically measures the mean circulatio$_{10}\rangle$n under perpendicular wind, is shown to decrease pedestrian-level concentrations (Fig. 10). Similar behaviour between $\langle$PM and $\langle$MKE$\rangle$ is observed also when focusing only on concentrations on the pavements, except that the relationship is slightly weaker (see Fig. S11 ans S12). Furthermore, results are also alike for N_{tot} (see Figs. S13–16).

The relationship of $\langle$TKE$\rangle$ and $\langle PM_{10} \rangle$ is more complicated (Fig. 12). In general, trees decrease TKE as also shown in Santiago et al. (2019). No linear relationship between $\langle$TKE$\rangle$ and $\langle PM_{10} \rangle$ can be observed with parallel wind, whereas with perpendicular wind $\langle PM_{10} \rangle$ is shown to systematically decrease with increasing $\langle$TKE$\rangle$. With parallel wind, $\langle$TKE$\rangle$ is clearly highest in S2C and around threefold compared to S0 at $z = 14.6$ m, which corresponds to the highest $\langle F_{bin6} \rangle$ values (Fig. 9a). Thus, with both wind conditions trees create mechanical turbulence and convert mean flow kinetic energy to the energy of the turbulent flow. Also in other scenarios with trees, $\langle$TKE$\rangle$ becomes larger than in S0 at $z =$

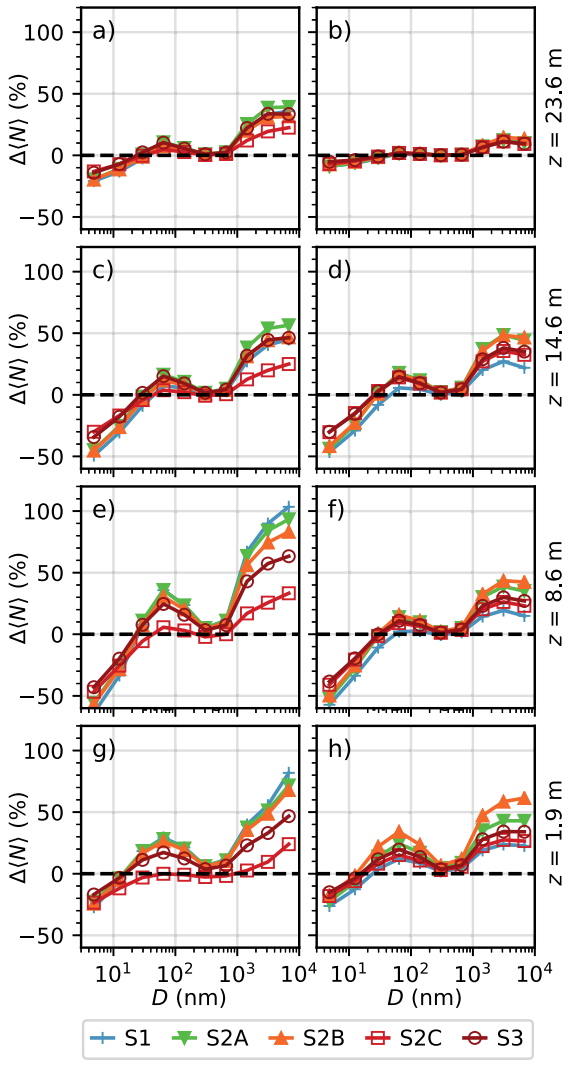

Fig. 8. Relative difference in the mean aerosol number concentration $\Delta\langle N\rangle$ (%) for different tree-layout scenarios compared to baseline scenario S0 as a function of geometric mean diameter $\overline{D}_g$ (nm) at different levels z with parallel (WD = 8°, left column: a, c, e, g) and perpendicular (WD = 82°, right column: b, d, f, h) wind. $\langle\ldots\rangle$ denotes the average over the whole boulevard.

14.6 m. Interestingly, ⟨TKE⟩ is constantly highest in S0 with perpendicular wind.

4. Discussion

The few previous CFD studies combining the aerodynamic impact of vegetation and dry deposition agree with our result that the dry deposition has a minor effect on aerosol concentrations compared to the aerodynamic impact. Here, we show a mean increase of 69–88%, 33–42% and 15–21% for PM_{10}, $PM_{2.5}$ and N_{tot} on the pavements, respectively, which falls within the wide range of those of previous studies (Abhijith et al., 2017). Moreover, a nearly linear relationship between PM_{10} and CVF has also been reported by Gromke et al. (2016) using neighbourhood-averaged normalised concentrations at z = 2 m. In our case the linearity was less pronounced. The hedges in S2B lead to on average 5–7% lower pedestrian-level concentrations over pavements compared to S2A, which corresponds to previous findings in Vos et al. (2013) and Gromke and Ruck (2012) also including dry deposition. On the contrary, Gromke et al. (2016) showed opposing results with discontinuous hedge rows. Nevertheless, the results are not fully comparable given the site-specific impacts of vegetation configuration as well as the inclusion of size-dependent deposition velocity and also the outperformance of LES compared to RANS.

Of the studies scenarios, the most efficient mitigation method for pedestrian-level aerosol mass concentrations over pavements is variable tree height in the middle and outermost rows of trees (scenario S2C) and for aerosol number four rows of trees (S1). Based on our results, S2C optimises the ventilation of the boulevard by the mean flow when wind is perpendicular to the street and by turbulence when wind is parallel to the street. Thus, we claim that slightly different processes control the street-canyon ventilation with different wind conditions. In general, with parallel wind, trees increase the turbulent transport of aerosol particles in the street canyon whereas with perpendicular wind, trees

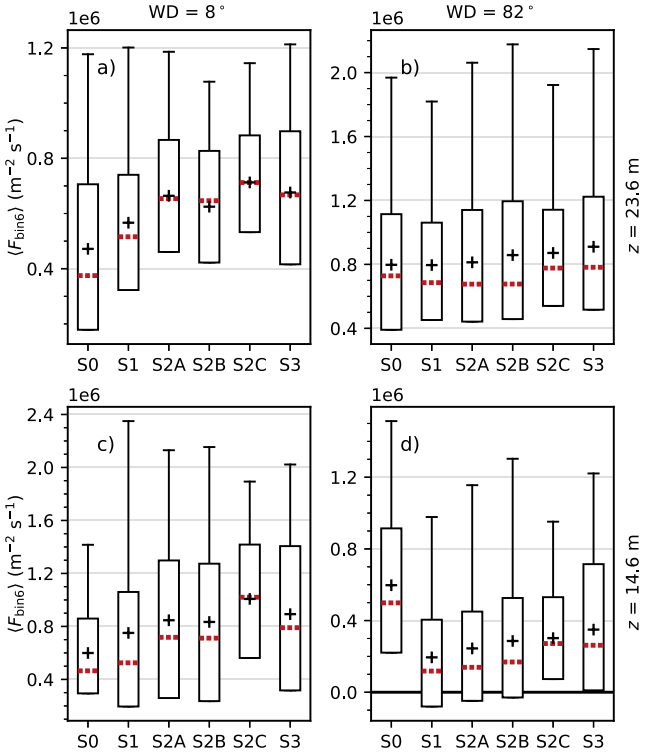

Fig. 9. Hourly vertical turbulent fluxes of aerosol size bin 6 $\langle F_{bin6}\rangle$ ($m^{-2}s^{-1}$, geometric mean diameter $\overline{D}_g$ = 303.3 nm) averaged over the whole boulevard with parallel (WD = 8°, left column: a, c) and perpendicular (WD = 82°, right column: b, d) wind. Flux is calculated at two heights: z = 14.6 m and z = 23.6 m. Black plus signs are mean values, red dashed lines medians, the lower and upper limit of the boxes 25th and 75th percentiles and whiskers the 95th percentiles. Notice the different y-axis in the subplots. $\langle\ldots\rangle$ denotes the average over the whole boulevard. (For interpretation of the references to colour in this figure legend, the reader is referred to the Web version of this article.)

Table 6
Relative difference in hourly mean (median in brackets) $\langle F_{bin6}\rangle$ (%) compared to S0 over the whole boulevard at z = 14.6 m and z = 23.6 m. $\langle\ldots\rangle$ denotes the average over the whole boulevard.

Wind direction	z (m)	S1	S2A	S2B	S2C	S3
Parallel (8°)	14.6	+14 (+3)	+38 (+45)	+37 (+45)	+70 (+110)	+43 (+55)
	23.6	+15 (+26)	+38 (+62)	+30 (+61)	+48 (+77)	+36 (+61)
Perpendicular (82°)	14.6	−65 (−76)	−59 (−73)	−51 (−66)	−50 (−47)	−44 (−50)
	23.6	+3 (−2)	+1 (−9)	+6 (−9)	+7 (+5)	+9 (+3)

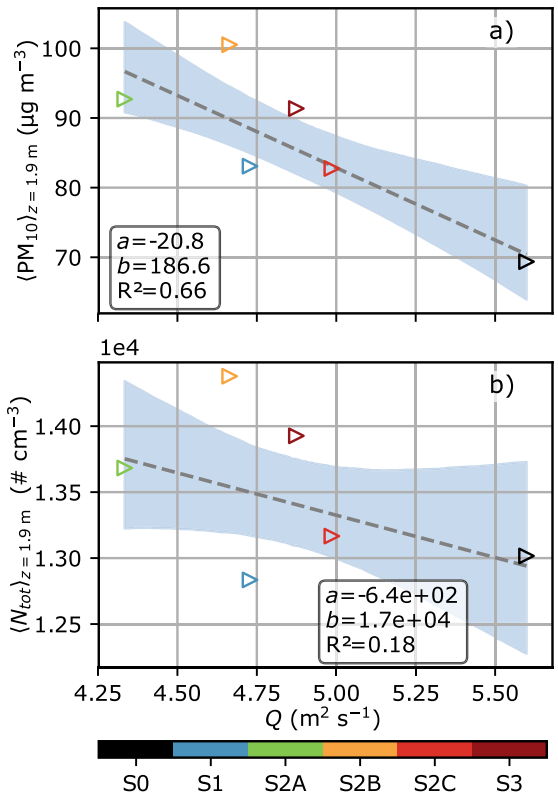

Fig. 10. Hourly a) $\langle PM_{10} \rangle$ (μg m^{-3}) and b) $\langle N_{tot} \rangle$ (# cm^{-3}) averaged over the whole boulevard at the pedestrian-level as a function of Q (the volumetric flow rate across the street canyon per unit length) for perpendicular wind conditions. The grey dashed lines are linear least squares fits and the blue areas represent the 95% confidence intervals of the fitted lines obtained using the bootstrap method with 10,000 bootstrap samples. ⟨…⟩ denotes the average over the whole boulevard. (For interpretation of the references to colour in this figure legend, the reader is referred to the Web version of this article.)

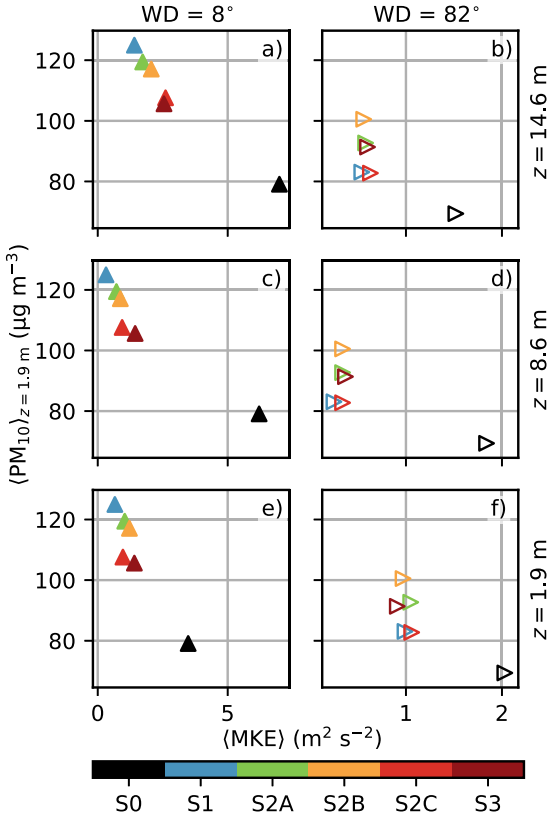

Fig. 11. The relationship between the mean kinetic energy ⟨MKE⟩ (m^2 s^{-2}) at different heights and $\langle PM_{10} \rangle$ (μg m^{-3}) at $z = 1.9$ m averaged over the whole boulevard with parallel (WD = 8°, left column: a, c, e) and perpendicular (WD = 82°, right column: b, d, f) wind. ⟨…⟩ denotes the average over the whole boulevard.

disturb the natural ventilation of the street canyon. Besides ventilation, the highest CVF in S1 results in the most effective dry deposition and lowest number concentrations. In addition to hedges in S2B, results on S2C indicates that lowering the vegetation mass closer to the emission source can be beneficial for ventilation and/or dry deposition.

In all scenarios, dry deposition is observed to be important only for smallest particles. This was also shown in Tong et al. (2016), which investigated the impact of roadside vegetation barriers on pollutant dispersion and dry deposition. However, both this study and Tong et al. (2016) used the parametrisation by Zhang et al. (2001), which is claimed to overestimate dry deposition for submicron aerosol particles (Petroff and Zhang, 2010). Hence, more sensitivity tests as well as further work to improve the parametrisations, especially in local scale modelling, is required.

As for the quantitative analysis, the modelled situation represents a dry, spring-time morning rush hour in an urban neighbourhood in a northern country, where studded tyres are applied in winter. These initial conditions lead to high PM_{10} concentrations with peaks >300 μg m^{-3}, which are up to 6–7-fold compared to $PM_{2.5}$. Nevertheless, the hourly averages are comparable with generally observed values (Kauhaniemi et al., 2011).

One of the main limitations of the study stems from the number of scenarios and inflow conditions investigated, which is restricted by the computational resources. Previous CFD studies have mainly applied RANS, which can be several orders of magnitude less expensive than LES. Still, we chose LES for its outperformance over RANS especially in urban areas (Tominaga and Stathopoulos, 2011). Given the computational costs of roughly 1000 CPU days per simulation (Section 2.3), we chose not to include any additional street-tree layouts above the realistic-ones given by the City of Helsinki. The limited number of scenarios limits the generalisation of the results with a wide range of street-tree layouts. Also, this study focused on the aerodynamic impact of trees on the flow, neglecting their shading and thermal impact. Also the biogenic volatile organic compounds are not considered and they will complicate the situation further by participating to aerosol particle formation and growth. Furthermore, vehicle-induced turbulence (VIT) is omitted as no efficient VIT parametrisation for neighbourhood-scale LES is currently available.

5. Conclusions

The purpose of this study was to understand the net effect of street trees on pedestrian-level aerosol particle metrics in a boulevard-type street canyon, and to find out which of the studied street-tree layout scenario minimises the concentrations over pavements and maximises vertical transport in the boulevard. We use the large-eddy simulation model PALM which allows treatment of permeable trees and includes a detailed aerosol particle module allowing for diameter-dependent dry deposition on vegetation and other surfaces. Two different wind directions, parallel and perpendicular to the boulevard, are examined.

Introducing trees to the street canyon increases aerosol mass concentrations over the pavements (PM_{10} by 4–123% and $PM_{2.5}$ by 1–72%) which to some degree is found to correlate with the relative volume of total vegetation (CVF) in the street canyon. Also, the aerosol number concentrations mainly increase (-14–53%) but as smallest particles have the highest deposition velocities, even a negative relationship with CVF

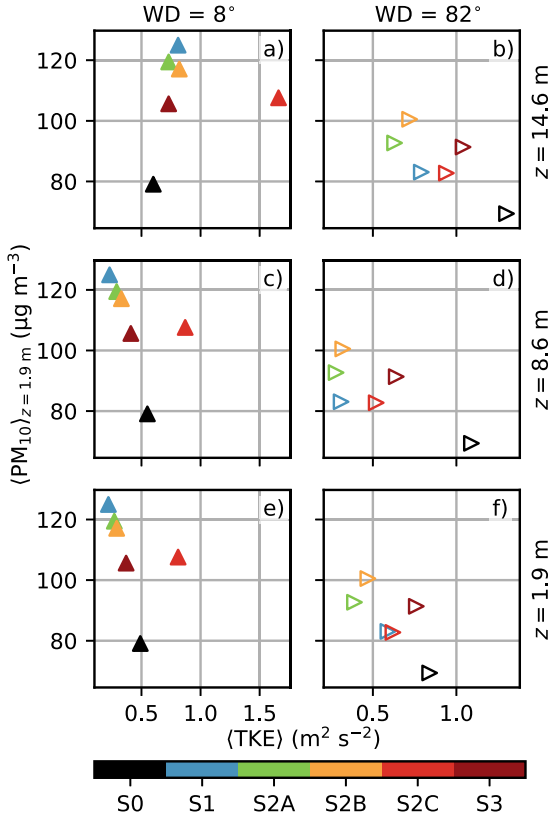

Fig. 12. The relationship between the turbulent kinetic energy ⟨TKE⟩) $m^2\ s^{-2}$) at different heights and ⟨PM_{10}⟩ (μg m^{-3}) at $z = 1.9$ m averaged over the whole boulevard with parallel (WD = 8°, left column: a, c, e) and perpendicular (WD = 82°, right column: b, d, f) wind. ⟨…⟩ denotes the average over the whole boulevard.

can be observed. Up to 50% lower number concentrations of the smallest aerosol size bins are observed at pedestrian-level when trees are present in the street space. These contradictory results for different aerosol sizes emphasise the importance of taking into account size-dependent dry deposition velocities and analysing also the smallest particles, which are the most harmful. Trees in the street space weaken the natural ventilation of the boulevard with wind perpendicular to the boulevard which can be seen as reduced circulation of the canyon vortex and MKE. At the same time, trees enhance TKE and the vertical turbulent transport of aerosol particles also well above the roof level with parallel wind. The influence is opposite within the street canyon and very minor above the roof level with perpendicular wind.

Of all scenarios with trees, the lowest mass concentrations over pavements are observed in S2C (three rows of trees with smaller outermost trees) with parallel wind and S1 (four rows of trees) with perpendicular wind. For aerosol number, lowest concentrations are observed in S1. Generally, S2C displays smallest concentration variability as well as highest vertical turbulent transport and TKE, but also weakest dry deposition. Hedges below the outermost rows of trees in S2B were not shown significant (5–7% decrease) for the pedestrian-level aerosol particle concentrations over pavements.

This study demonstrates how LES can be used to aid urban planning when designing new and developing present neighbourhoods. Including permeable vegetation and size-dependent dry deposition will provide more realistic description of the mechanisms of urban form in contributing to local air pollution distributions. The results obtained in this study are not directly transferable to all kinds of urban vegetation but rather only to those on wide boulevard type street canyons. More work in future is needed to comprehensively understand the complex nature of urban vegetation.

Code and data availability

This study applied the PALM model system version 6.0 revision 3698, which is openly available on https://palm.muk.uni-hannover.de (last access: 28.11.2019) under the terms of the GNU General Public License (v3). The exact version of the model code can be downloaded from https://doi.org/10.5281/zenodo.3556317 and the input data from https://doi.org/10.5281/zenodo.3556287 (Karttunen and Kurppa, 2019).

Competing interests

The authors declare that they have no conflict of interest.

Declaration of competing interest

The authors declare that they have no known competing financial interests or personal relationships that could have appeared to influence the work reported in this paper.

CRediT authorship contribution statement

Sasu Karttunen: Methodology, Software, Formal analysis, Investigation, Resources, Data curation, Visualization, Writing - original draft, Writing - review & editing. **Mona Kurppa:** Conceptualization, Methodology, Software, Formal analysis, Visualization, Writing - original draft, Writing - review & editing. **Mikko Auvinen:** Methodology, Software, Writing - review & editing. **Antti Hellsten:** Methodology, Writing - review & editing. **Leena Järvi:** Conceptualization, Methodology, Writing - original draft, Writing - review & editing, Supervision, Funding acquisition.

Acknowledgements

We thank Helsinki Metropolitan Region Urban Research Program, the Academy of Finland Centre of Excellence (no. 307331) and PROFI3, Project Smart urban solutions for air quality, disasters and city growth (SMURBS) funded by ERA-NET-COFUND project under ERA-PLANET, and Atmospheric mathematics program (ATMATH) and Doctoral programme in Atmospheric Sciences (ATM-DP) of the University of Helsinki. The City of Helsinki is acknowledged for their contribution in planning the analysed street-tree layout scenarios.

Appendix A. Supplementary data

Supplementary data to this article can be found online at https://doi.org/10.1016/j.aeaoa.2020.100073.

References

Abhijith, K., Kumar, P., Gallagher, J., McNabola, A., Baldauf, R., Pilla, F., Broderick, B., Sabatino, S.D., Pulvirenti, B., 2017. Air pollution abatement performances of green infrastructure in open road and built-up street canyon environments – a review. Atmos. Environ. 162, 71–86. https://doi.org/10.1016/j.atmosenv.2017.05.014.

Auvinen, M., Boi, S., Hellsten, A., Tanhuanpää, T., Järvi, L., 2020. Study of realistic urban boundary layer turbulence with high-resolution large-eddy simulation. Atmosphere 11, 201. https://doi.org/10.3390/atmos11020201.

Barlow, J.F., Harman, I.N., Belcher, S.E., 2004. Scalar fluxes from urban street canyons. Part I: laboratory simulation. Bound.-Lay. Meteorol. 113, 369–385. https://doi.org/10.1007/s10546-004-6204-8.

Britter, R.E., Hanna, S.R., 2003. Flow and dispersion in urban areas. Annu. Rev. Fluid Mech. 35, 469–496. https://doi.org/10.1146/annurev.fluid.35.101101.161147.

Buccolieri, R., Gromke, C., Sabatino, S.D., Ruck, B., 2009. Aerodynamic effects of trees on pollutant concentration in street canyons. Sci. Total Environ. 407, 5247–5256. https://doi.org/10.1016/j.scitotenv.2009.06.016.

Buccolieri, R., Salim, S.M., Leo, L.S., Sabatino, S.D., Chan, A., Ielpo, P., de Gennaro, G., Gromke, C., 2011. Analysis of local scale tree–atmosphere interaction on pollutant

concentration in idealized street canyons and application to a real urban junction. Atmos. Environ. 45, 1702–1713. https://doi.org/10.1016/j.atmosenv.2010.12.058.
Chen, L., Hang, J., Sandberg, M., Claesson, L., Sabatino, S.D., Wigo, H., 2017. The impacts of building height variations and building packing densities on flow adjustment and city breathability in idealized urban models. Build. Environ. 118, 344–361. https://doi.org/10.1016/j.buildenv.2017.03.042.
City of Helsinki, 2016. Helsinki city plan 2016. last access 18 December 2018. URL. http://www.yleiskaava.fi/en/city-plan/.
Fenger, J., 2009. Air pollution in the last 50 years–from local to global. Atmos. Environ. 43, 13–22. https://doi.org/10.1016/j.atmosenv.2008.09.061.
Finnish Meteorological Institute. Weather observations: Kaisaniemi. last access 21 august 2018. URL. http://catalog.fmi.fi/geonetwork/srv/eng/catalog.search#/metadata/228310f3-12a3-43f6-9949-7ee27dc9b047.
Giometto, M., Christen, A., Egli, P., Schmid, M., Tooke, R., Coops, N., Parlange, M., 2017. Effects of trees on mean wind, turbulence and momentum exchange within and above a real urban environment. Adv. Water Resour. 106, 154–168. https://doi.org/10.1016/j.advwatres.2017.06.018 (tribute to Professor Garrison Sposito: An Exceptional Hydrologist and Geochemist).
Gousseau, P., Blocken, B., Stathopoulos, T., van Heijst, G., 2011. CFD simulation of near-field pollutant dispersion on a high-resolution grid: a case study by LES and RANS for a building group in downtown Montreal. Atmos. Environ. 45, 428–438. https://doi.org/10.1016/j.atmosenv.2010.09.065.
Gromke, C., Blocken, B., 2015. Influence of avenue-trees on air quality at the urban neighborhood scale. part ii: traffic pollutant concentrations at pedestrian level. Environ. Pollut. 196, 176–184. https://doi.org/10.1016/j.envpol.2014.10.015.
Gromke, C., Jamarkattel, N., Ruck, B., 2016. Influence of roadside hedgerows on air quality in urban street canyons. Atmos. Environ. 139, 75–86. https://doi.org/10.1016/j.atmosenv.2016.05.014.
Gromke, C., Ruck, B., 2012. Pollutant concentrations in street canyons of different aspect ratio with avenues of trees for various wind directions. Bound.-Lay. Meteorol. 144, 41–64. https://doi.org/10.1007/s10546-012-9703-z.
Gronemeier, T., Sühring, M., 2019. On the effects of lateral openings on courtyard ventilation and pollution—a large-eddy simulation study. Atmosphere 10. https://doi.org/10.3390/atmos10020063.
Hackbusch, W., 1985. Multi-grid Methods and Applications, 1 ed. Springer, Berlin, Germany. https://doi.org/10.1007/978-3-662-02427-0.
Hall, D., Walker, S., Spanton, A., 1999. Dispersion from courtyards and other enclosed spaces. Atmos. Environ. 33, 1187–1203. https://doi.org/10.1016/S1352-2310(98)00284-2.
Hang, J., Li, Y., Sandberg, M., Buccolieri, R., Sabatino, S.D., 2012. The influence of building height variability on pollutant dispersion and pedestrian ventilation in idealized high-rise urban areas. Build. Environ. 56, 346–360. https://doi.org/10.1016/j.buildenv.2012.03.023.
Irga, P., Burchett, M., Torpy, F., 2015. Does urban forestry have a quantitative effect on ambient air quality in an urban environment? Atmos. Environ. 120, 173–181. https://doi.org/10.1016/j.atmosenv.2015.08.050.
Janhäll, S., 2015. Review on urban vegetation and particle air pollution – deposition and dispersion. Atmos. Environ. 105, 130–137. https://doi.org/10.1016/j.atmosenv.2015.01.052 iD: 271798.
Jeanjean, A., Monks, P., Leigh, R., 2016. Modelling the effectiveness of urban trees and grass on PM2.5 reduction via dispersion and deposition at a city scale. Atmos. Environ. 147, 1–10. https://doi.org/10.1016/j.atmosenv.2016.09.033.
Jeanjean, A.P., Buccolieri, R., Eddy, J., Monks, P.S., Leigh, R.J., 2017. Air quality affected by trees in real street canyons: the case of Marylebone neighbourhood in central London. Urban For. Urban Gree 22, 41–53. https://doi.org/10.1016/j.ufug.2017.01.009.
Kanani, F., Träumner, K., Ruck, B., Raasch, S., 2014. What determines the differences found in forest edge flow between physical models and atmospheric measurements? – an LES study. Meteorol. Z. 23, 33–49. https://doi.org/10.1127/0941-2948/2014/0542.
Karttunen, S., Kurppa, M., 2019. Input Data for Article "Large Eddy Simulation of the Optimal Street-Tree Layout for Pedestrian-Level Aerosol Particle Concentrations". https://doi.org/10.5281/zenodo.3556287.
Katul, G.G., Mahrt, L., Poggi, D., Sanz, C., 2004. ONE- and TWO-equation models for canopy turbulence. Boundary-Layer Meteorol. 81 https://doi.org/10.1023/B:BOUN.0000037333.48760.e5.
Kauhaniemi, M., Kukkonen, J., Härkonen, J., Nikmo, J., Kangas, L., Omstedt, G., Ketzel, M., Kousa, A., Haakana, M., Karppinen, A., 2011. Evaluation of a road dust suspension model for predicting the concentrations of PM10 in a street canyon. Atmos. Environ. 45, 3646–3654. https://doi.org/10.1016/j.atmosenv.2011.04.055.
Kokkola, H., Korhonen, H., Lehtinen, K.E.J., Makkonen, R., Asmi, A., Järvenoja, S., Anttila, T., Partanen, A.I., Kulmala, M., Järvinen, H., Laaksonen, A., Kerminen, V.M., 2008. Salsa - a sectional aerosol module for large scale applications. Atmos. Chem. Phys. 8, 2469–2483. https://doi.org/10.5194/acp-8-2469-2008.
Kurppa, M., Hellsten, A., Raasch, S., Vesala, T., Järvi, L., 2018. Ventilation and air quality in city blocks using large-eddy simulation—urban planning perspective. Atmosphere 9, 65. https://doi.org/10.3390/atmos9020065.
Kurppa, M., Hellsten, A., Roldin, P., Kokkola, H., Tonttila, J., Auvinen, M., Kent, C., Kumar, P., Maronga, B., Järvi, L., 2019. Implementation of the sectional aerosol module SALSA2.0 into the PALM model system 6.0: model development and first evaluation. Geosci. Model Dev. (GMD) 12, 1403–1422. https://doi.org/10.5194/gmd-12-1403-2019.
Letzel, M.O., Krane, M., Raasch, S., 2008. High resolution urban large-eddy simulation studies from street canyon to neighbourhood scale. Atmos. Environ. 42, 8770–8784. https://doi.org/10.1016/j.atmosenv.2008.08.001.
Lin, M., Hang, J., Li, Y., Luo, Z., Sandberg, M., 2014. Quantitative ventilation assessments of idealized urban canopy layers with various urban layouts and the same building packing density. Build. Environ. 79, 152–167. https://doi.org/10.1016/j.buildenv.2014.05.008.
Lindberg, F., Thorsson, S., Rayner, D., Lau, K., 2016. The impact of urban planning strategies on heat stress in a climate-change perspective. Sustain. Cities Soc. 25, 1–12. https://doi.org/10.1016/j.scs.2016.04.004.
Maronga, B., Banzhaf, S., Burmeister, C., Esch, T., Forkel, R., Fröhlich, D., Fuka, V., Gehrke, K.F., Geletič, J., Giersch, S., Gronemeier, T., Groß, G., Heldens, W., Hellsten, A., Hoffmann, F., Inagaki, A., Kadasch, E., Kanani-Sühring, F., Ketelsen, K., Khan, B.A., Knigge, C., Knoop, H., Krč, P., Kurppa, M., Maamari, H., Matzarakis, A., Mauder, M., Pallasch, M., Pavlik, D., Pfafferott, J., Resler, J., Rissmann, S., Russo, E., Salim, M., Schrempf, M., Schwenkel, J., Seckmeyer, G., Schubert, S., Sühring, M., von Tils, R., Vollmer, L., Ward, S., Witha, B., Wurps, H., Zeidler, J., Raasch, S., 2019. Overview of the PALM model system 6.0. Geosci. Model Dev. Discuss. (GMDD) 1–63. https://doi.org/10.5194/gmd-2019-103.
Maronga, B., Gryschka, M., Heinze, R., Hoffmann, F., Kanani-Sühring, F., Keck, M., Ketelsen, K., Letzel, M.O., Sühring, M., Raasch, S., 2015. The parallelized large-eddy simulation model (PALM) version 4.0 for atmospheric and oceanic flows: model formulation, recent developments, and future perspectives. Geosci. Model Dev. (GMD) 8, 2515–2551. https://doi.org/10.5194/gmd-8-2515-2015.
Mayhead, G.J., 1973. Some drag coefficients for british forest trees derived from wind tunnel studies. Agric. Meteorol. 12, 123–130. https://doi.org/10.1016/0002-1571(73)90013-7.
Moradpour, M., Afshin, H., Farhanieh, B., 2017. A numerical investigation of reactive air pollutant dispersion in urban street canyons with tree planting. Atmos. Pollut. Res. 8, 253–266. https://doi.org/10.1016/j.apr.2016.09.002.
Munters, W., Meneveau, C., Meyers, J., 2016. Shifted periodic boundary conditions for simulations of wall-bounded turbulent flows. Phys. Fluids 28, 025112. https://doi.org/10.1063/1.4941912.
Nel, A., Xia, T., Mädler, L., Li, N., 2006. Toxic potential of materials at the nanolevel. Science 311, 622–627. https://doi.org/10.1126/science.1114397.
Niemelä, J., Saarela, S.R., Söderman, T., Kopperoinen, L., Yli-Pelkonen, V., Väre, S., Kotze, D.J., 2010. Using the ecosystem services approach for better planning and conservation of urban green spaces: a Finland case study. Biodivers. Conserv. 19, 3225–3243. https://doi.org/10.1007/s10531-010-9888-8.
Nosek, Š., Kukačka, L., Kellnerová, R., Jurčáková, K., Jaňour, Z., 2016. Ventilation processes in a three-dimensional street canyon. Bound.-Lay. Meteorol. 159, 259–284. https://doi.org/10.1007/s10546-016-0132-2.
Park, S.B., Baik, J.J., Raasch, S., Letzel, M.O., 2012. A large-eddy simulation study of thermal effects on turbulent flow and dispersion in and above a street canyon. J. Appl. Meteorol. Clim. 51, 829–841. https://doi.org/10.1175/JAMC-D-11-0180.1.
Petroff, A., Zhang, L., 2010. Development and validation of a size-resolved particle dry deposition scheme for application in aerosol transport models. Geosci. Model Dev. (GMD) 3, 753–769. https://doi.org/10.5194/gmd-3-753-2010.
Ramponi, R., Blocken, B., de Coo, L.B., Janssen, W.D., 2015. Cfd simulation of outdoor ventilation of generic urban configurations with different urban densities and equal and unequal street widths. Build. Environ. 92, 152–166. https://doi.org/10.1016/j.buildenv.2015.04.018.
Raupach, M.R., Finnigan, J.J., Brunei, Y., 1996. Coherent eddies and turbulence in vegetation canopies: the mixing-layer analogy. Bound.-Lay. Meteorol. 78, 351–382. https://doi.org/10.1007/BF00120941.
Razak, A.A., Hagishima, A., Ikegaya, N., Tanimoto, J., 2013. Analysis of airflow over building arrays for assessment of urban wind environment. Build. Environ. 59, 56–65. https://doi.org/10.1016/j.buildenv.2012.08.007.
Requia, W.J., Mohamed, M., Higgins, C.D., Arain, A., Ferguson, M., 2018. How clean are electric vehicles? Evidence-based review of the effects of electric mobility on air pollutants, greenhouse gas emissions and human health. Atmos. Environ. 185, 64–77. https://doi.org/10.1016/j.atmosenv.2018.04.040.
Salim, S.M., Buccolieri, R., Chan, A., Sabatino, S.D., 2011. Numerical simulation of atmospheric pollutant dispersion in an urban street canyon: comparison between RANS and LES. J. Wind Eng. Ind. Aerod. 99, 103–113. https://doi.org/10.1016/j.jweia.2010.12.002.
Santiago, J., Borge, R., Martin, F., de la Paz, D., Martilli, A., Lumbreras, J., Sanchez, B., 2017a. Evaluation of a CFD-based approach to estimate pollutant distribution within a real urban canopy by means of passive samplers. Sci. Total Environ. 576, 46–58. https://doi.org/10.1016/j.scitotenv.2016.09.234.
Santiago, J.L., Buccolieri, R., Rivas, E., Sanchez, B., Martilli, A., Gatto, E., Martín, F., 2019. On the impact of trees on ventilation in a real street in Pamplona, Spain. Atmosphere 10. https://doi.org/10.3390/atmos10110697.
Santiago, J.L., Martilli, A., Martin, F., 2017b. On dry deposition modelling of atmospheric pollutants on vegetation at the microscale: application to the impact of street vegetation on air quality. Bound.-Lay. Meteorol. 162, 451–474. https://doi.org/10.1007/s10546-016-0210-5.
Tallis, M., Taylor, G., Sinnett, D., Freer-Smith, P., 2011. Estimating the removal of atmospheric particulate pollution by the urban tree canopy of london, under current and future environments. Landsc. Urban Plann. 103, 129–138. https://doi.org/10.1016/j.landurbplan.2011.07.003.
Tanhuanpää, T., Vastaranta, M., Kankare, V., Holopainen, M., Hyyppä, J., Hyyppä, H., Alho, P., Raisio, J., 2014. Mapping of urban roadside trees – a case study in the tree register update process in Helsinki City. Urban For. Urban Gree. 13, 562–570. https://doi.org/10.1016/j.ufug.2014.03.005.
Tominaga, Y., Stathopoulos, T., 2011. CFD modeling of pollution dispersion in a street canyon: comparison between LES and RANS. J. Wind Eng. Ind. Aerod. 99, 340–348. https://doi.org/10.1016/j.jweia.2010.12.005.

Tong, Z., Baldauf, R.W., Isakov, V., Deshmukh, P., Zhang, K.M., 2016. Roadside vegetation barrier designs to mitigate near-road air pollution impacts. Sci. Total Environ. 541, 920–927. https://doi.org/10.1016/j.scitotenv.2015.09.067.

Vollsinger, S., Mitchell, S.J., Byrne, K.E., Novak, M.D., Rudnicki, M., 2005. Wind tunnel measurements of crown streamlining and drag relationships for several hardwood species. Can. J. For. Res. 35, 1238–1249. https://doi.org/10.1139/x05-051.

Vos, P.E., Maiheu, B., Vankerkom, J., Janssen, S., 2013. Improving local air quality in cities: to tree or not to tree? Environ. Pollut. vol. 183, 113–122. https://doi.org/10.1016/j.envpol.2012.10.021. Selected Papers from Urban Environmental Pollution 2012.

Vranckx, S., Vos, P., Maiheu, B., Janssen, S., 2015. Impact of trees on pollutant dispersion in street canyons: a numerical study of the annual average effects in Antwerp, Belgium. Sci. Total Environ. 532, 474–483. https://doi.org/10.1016/j.scitotenv.2015.06.032.

Vtt, 2018. Lipasto Unit Emissions -database. technical research centre of finland ltd. last access 17 september 2018. URL: lipasto.vtt.fi/yksikkopaastot/.

Wang, Y.J., Nguyen, M.T., Steffens, J.T., Tong, Z., Wang, Y., Hopke, P.K., Zhang, K.M., 2013. Modeling multi-scale aerosol dynamics and micro-environmental air quality near a large highway intersection using the CTAG model. Sci. Total Environ. 443, 375–386. https://doi.org/10.1016/j.scitotenv.2012.10.102.

Wang, Y.J., Zhang, K.M., 2012. Coupled turbulence and aerosol dynamics modeling of vehicle exhaust plumes using the CTAG model. Atmos. Environ. 59, 284–293. https://doi.org/10.1016/j.atmosenv.2012.04.062.

Wania, A., Bruse, M., Blond, N., Weber, C., 2012. Analysing the influence of different street vegetation on traffic-induced particle dispersion using microscale simulations. J. Environ. Manag. 94, 91–101. https://doi.org/10.1016/j.jenvman.2011.06.036.

Wicker, L.J., Skamarock, W.C., 2002. Time-splitting methods for elastic models using forward time schemes. Mon. Weather Rev. 130, 2088–2097. https://doi.org/10.1175/1520-0493(2002)130<2088:TSMFEM>2.0.CO;2.

Williamson, J.H., 1980. Low-storage Runge-Kutta schemes. J. Comput. Phys. 35, 48–56. https://doi.org/10.1016/0021-9991(80)90033-9.

Xie, Z., Castro, I., 2006. LES and RANS for turbulent flow over arrays of wall-mounted obstacles. Flow, Turbul. Combust. 76, 291–312. https://doi.org/10.1007/s10494-006-9018-6.

Yuan, C., Ng, E., Norford, L.K., 2014. Improving air quality in high-density cities by understanding the relationship between air pollutant dispersion and urban morphologies. Build. Environ. 71, 245–258. https://doi.org/10.1016/j.buildenv.2013.10.008.

Zhang, L., Gong, S., Padro, J., Barrie, L., 2001. A size-segregated particle dry deposition scheme for an atmospheric aerosol module. Atmos. Environ. 35, 549–560. https://doi.org/10.1016/S1352-2310(00)00326-5.

Zhang, Y., Seigneur, C., Seinfeld, J.H., Jacobson, M.Z., Binkowski, F.S., 1999. Simulation of aerosol dynamics: a comparative review of algorithms used in air quality models. Aerosol Sci. Technol. 31, 487–514. https://doi.org/10.1080/027868299304039.